ENGINEERING TECHNICAL REPORT

NOX

THE LOAD CARRYING CAPACITY AND STABILITY OF HYBRID GAS BEARINGS

by

L.W. Winn
B. Sternlicht

R62AT8

March 11, 1962

AIRCRAFT ACCESSORY TURBINE DEPARTMENT

GENERAL ELECTRIC

APPLIED MECHANICS AND SYSTEMS ANALYSIS LABORATORY

THE LOAD CARRYING CAPACITY AND STABILITY OF HYBRID GAS BEARINGS

by

L.W. Winn
B. Sternlicht*

MARCH 11, 1962

TECHNICAL REPORT R62AT8

FOR: Office of Naval Research
CONTRACT NO.: NONR 2844(00)
TASK NO.: NR097-348

*Presently associated with
Mechanical Technology Incorporated
Latham, New York

DISTRIBUTION

Complete Report:

AATD Library, 3-74
SAE Library, 2-40
FPD Library, Evendale
TIS, Bldg. 5, Schenectady

Schenectady, New York
RC Elwell, 37-323
GR Fox, 37-1020
LE St. Pierre, 4A16, Res. Lab.
JD McHugh, 37-1020
DW Jones, 37-1020
WR Nial, 37-304
RM Mains, 37-680
FJ Martin, 5A6, Res. Lab.
GM Rentzepis, 37-680

Bridgeport, Connecticut
CA Edman, Fan Dept.

Lynn River Works
MA Prohl, 2-64G
JD Cairns, 3-74
LW Winn, 3-74 (2)

Fitchburg, Massachusetts
AE Truran, SST

Erie, Pennsylvania
PS Potts, DCM & G

Ft. Wayne, Indiana
RW Dochterman, CP Div., Lab. Op.

San Jose, California
K. Cohen, APED

Pittsfield, Massachusetts
DF Wilcock, Ordnance

Title Page:

TIS, Bldg. 5, Schenectady

TABLE OF CONTENTS

GLOSSARY OF TERMS

Self-acting - (Used interchangeably with hydredynamic) - a bearing system in which the journal and bearing are separated by a fluid film resulting from pressures generated by relative displacement and motion of the surfaces.

Externally Pressurized - (Used interchangeably with hydrostatic) - a bearing system in which the journal is separated from the bearing by fluid film established due to introduction of pressurized fluid into the clearance between them.

Hybrid Bearings - A bearing system combining self acting and externally pressurized features.

Steady State Performance - A condition at which the fluid film pressure is distributed independently of time, i.e., stationary journal axis.

Dynamic Performance - A condition under which the axes of the journal moves so that local gas film pressures vary with time. Examples of dynamic operation are:

a. Start-up and shutdown transients

b. Motion excited by rotating load

c. Motion excited by reciprocating load

d. Bearing instability (H.F.W., F.F. W., and synchronous whirl as described in this paper)

Whirl Ratio - Ratio of frequency of shaft rotation to frequency of shaft whirl.

LIST OF SYMBOLS

L/D	Length/Diameter
b	m/w
c	Radial Clearance, 1 inch
f	Bearing Load, lbs.
I_P	Polar Moment of Inertia, #/sec.^{2}/in.
I_T	Translatory Moment of Inertia, #/sec.^{2}/in.
K_2	Radial Bearing Stiffness, #/inch
K_c	Radial Translatory Stiffness Evaluated at ω_c, #/inch
ω	Angular Velocity, rad./sec.
ω_c	Angular Velocity at Onset of H.F.W. - Conical Whip, rad/sec.
ω_T	Angular Velocity at Onset of H.F.W. - Translatory Whip, rad/sec.
ℓ	Bearing Span c-c, inches
L	Bearing Length, inches
m	Mass, $\frac{\#/\text{sec.}^2}{\text{inch}}$
P_a	Ambient Pressure, psia
R	Bearing Radius, inches
ϵ	Eccentricity Ratio
Λ	Compressibility Number
μ	Viscosity, $\frac{\#/\text{sec.}}{\text{in}^2}$
ω	Attitude Angle, degree
K_3	Radial Stiffness Under Misaligned Conditions
K_S	Static Spring Stiffener
F_{rh}	Radial Hydrodynamic Force
F_{th}	Tangential Hydrodynamic Force
e	Eccentricity - inches

I. INTRODUCTION

The theory of externally pressurized bearings, despite valuable contributions by some investigators, is still in its initial stages of evolution. Most of the solutions presently available (Refs. 1, 2, 3, 4, page 18) disregard rotational effects and as such can only be used with fair accuracy to determine the static load carrying capacity of externally pressurized bearings. However, since shaft rotation can have serious effects on the performance of externally pressurized bearings, it must be included in any analysis if the latter is to serve as a useful and reliable tool to the designer of systems utilizing hybrid (hydrodynamic-hydrostatic) gas bearings. The effects of rotation can be divided into two categories:

1. Effect of rotation on load carrying capacity and flow.
2. Effects of rotation on dynamic performance of a rotor-bearing system.

Regarding the first category, a recent theoretical analysis which includes the effects of rotation, shows that the hydrodynamic effect may or may not have a significant influence on the hydrostatic load capacity; its effect depends upon the operating conditions (Ref. 5, page 18). Effects of rotation on the dynamic behavior of the rotor-bearing system, however, can be quite severe and plagued by various types of instabilities which have been recognized and can broadly be defined as:

1. Critical Speed

   This is a rotating speed of a journal which corresponds to the resonant frequencies of the system. (The system critical speeds include rigid body as well as bending or torsional critical speeds).

2. Half-Frequency Whirl

A special case of instability generally associated with self-acting journal bearings. This instability occurs when the journal speed reaches a critical value. The journal axis whirls at a frequency of one-half or nearly one-half of the journal speed in the same direction as the journal rotation. The motion of the journal axis can be either conical or translatory.

3. Fractional-Frequency Whirl

The subject phenomenon is a special case of instability generally associated with hybrid journal bearings. This instability occurs when the journal speed reaches a critical value. The journal axis whirls at a frequency which is a fraction of the journal speed in the same direction as the journal rotation. The motion of the journal axis can be either conical or translatory. (The expression for the fractional frequency is given in equation 14, (page 15). and in the limit where self-acting forces predominate, it approaches the half-frequency whirl).

4. Pneumatic Hammer

This is a self-excited oscillation in the flow system of an externally pressurized bearing. This oscillation does not necessarily require shaft rotation.

II. TEST EQUIPMENT

Figure 1 presents a picture of the test rig which consists of a housing incorporating two journal bearings, the length of which can be changed up to 2 inches maximum. The shaft is 2 inches in diameter and accommodates a Terry-type impulse drive turbine on one end. The turbine employs full arc admission to minimize aerodynamic forces on the rotor. A dummy wheel is mounted on the other end of the rotor to provide rotor symmetry, decrease coastdown time, serve as a speed signal generating device, and a direction of rotation reverser.

The bearings (leaded-bronze) are externally fed through a total of eight orifices per bearing with all connections extending to a common manifold for each individual bearing. The orifice holder (figure 2, page 24) includes a removable orifice insert to facilitate quick orifice changes. In addition to the replaceable orifices, fixed orifices (.052 inch) are permanently incorporated in the journal bearing. This series orifice combination provides a means for changing the feeding system from orifice compensation to a combination of orifice-inherent compensation, or pure-inherent compensation through changes in replaceable orifice diameter and clearance.

Each bearing is fed via flowmeters shown in figure 1. The two meters shown for each bearing cover a range from 0 - 1.5 scfm with accuracy ranging from 2% - 8% of measured flow. Pressure gages calibrated to indicate absolute pressure with accuracy of $\pm$ .5 psi are used to register supply pressure levels.

Loading is accomplished through an air piston connected through a flexible foil to a 180° recessed gas journal bearing. The piston pulls against the foil which, in turn, applies a uniform load to the shaft. Since this system permits uniform

and indirect (through air film) load application, damping applied through the loading device which may effect onsets of instability can be considered negligible. Due to instability encountered on the loader bearing above 40,000 rpm, the use of the same had to be restricted to speeds below that level. The nature of this instability was not determined; however, it should be noted for future references that the bearing was 2 inches in diameter with 0.001 inch radial clearance and a recessed depth of 0.0005 inch, with 3/16 inch wide lands running around the entire perimeter. A centrally located 0.25 inch diameter hole was used to admit external air under pressure.

Each bearing end is supplied with four capacitive probes placed 90° apart with the output of each fed directly through proximity meters to a cathode-ray oscilloscope (CRO). Calibration of the CRO screen with the probe input permits determination of shaft position with accuracy of $\pm$ 25 x 10^{-6} inches or better. The same probe outputs are also used to determine frequency of oscillation, criticals and phase relationships between both ends.

Two thrust plates externally pressurized through 0 - 0.020 inch diameter orifices, as shown in figure 3, are used to contain the rotor in the axial direction. Total axial play amounts to 0.004 inch.

The entire unit is mounted on a heavy steel table which in turn is mounted on vibration isolation pads to reduce effects of building vibrations.

III. DISCUSSION OF TEST RESULTS

A. Instabilities

1. Criticals

In all tests described in this report, two critical speeds were observed in the safe operating speed range of the rotor. The lower critical corresponded to the conical mode. This conical whirl persisted up to the second critical. If one is to utilize the criterion for conical criticals described in Ref. 9 (page 18) then

$$\frac{\ell^2}{2} K_c + 2K_3 = \left(\frac{\omega_c}{n}\right)^2 \left(I_T - n I_p\right)$$

and where the critical frequency occurs at frequency of one per rev., n = 1 and

$$\frac{\ell^2}{2} K_c + 2K_3 = \omega_c^2 \left(I_T - I_p\right) \tag{1}$$

where K_3 is the radial stiffness under misaligned conditions, K_3 can be evaluated by making simplifying assumptions about end effects, and by assuming that each elemental length of the bearing contributes equally to the linear stiffness. Thus:

$$K_3 = \frac{L^2}{12} K_c \tag{2}$$

The translatory critical is a function of film stiffness and can be expressed as:

$$\omega_T^2 = \frac{2K_T}{m} \tag{3}$$

Substituting (2) in (1) and combining (1) and (3), one obtains the ratio of translatory to conical criticals for a two bearing system.

$$\frac{\omega_T^2}{\omega_c^2} = \frac{12\left(I_T - I_p\right) K_T}{m\left(3\ell^2 + L^2\right) K_c} \tag{4}$$

Assuming further that $K_T = K_c$ (i.e., the two criticals are not too far apart in speed and therefore the stiffnesses are not too different), then the ratio of criticals, knowing the translatory and polar moments of inertia, bearing span, bearing length, and mass of rotor can be easily computed from equation 4. For our case:

$$I_T = 0.612 \text{ \# sec.}^2 - \text{in.}$$

$$I_p = 0.0172 \text{ \# sec.}^2 - \text{in.}$$

$$m = 0.0341 \frac{\text{\#-sec.}^2}{\text{in.}}$$

$$l = 6.487 \text{ in.}$$

$$L = 1 \text{ in.}$$

and $\frac{\omega_T}{\omega_c} = 1.285$

Table I presents the test results in terms of criticals and onset of fractional-frequency whirl for all conditions observed. The lowest critical listed in column 3 corresponds to the conical mode induced by gyroscopic rotor effects (equation 1). Column 4 lists the next critical corresponding to the translatory mode (equation 3). Column 5 gives the onset of fractional-frequency whirl. Values of criticals for C = 0.0005 inch given in this table had to be calculated since the amplitude of vibration with this particular clearance was too low to permit accurate measurements. The ratio of criticals as given in column 6 varies between 1.235 - 1.65, and does not remain constant at 1.285 as calculated above and based on $K_T = K_c$. The variation appears to be a function of orifice size, clearance and pressure at conditions of constant load under which those tests were performed. Column 7 gives ratios of onset of fractional frequency whirl to lowest system critical.

A comparison between calculated values and test values of the conical and translatory criticals is given in Table 2. The calculated criticals are based on equation 3 where the film stiffness K_T has been obtained from test results on load carrying capacity at a given load of 6.57 lbs. per bearing. Theoretical values based upon the theoretically derived stiffness are also given. The test values obtained have then been reduced by a factor of 1.285 to yield calculated values of conical criticals. As can be seen, the correlation of calculated and test values for the translatory criticals is good. Only fair agreement exists between calculated and test values of conical criticals. This is probably due to the simplifying assumptions made in calculating the conical stiffness.

2. Pneumatic Hammer

The instability known as pneumatic hammer was encountered in one bearing geometry (L/D - .5, D = 2.00 inches, P_s = 120 psia, C = 0.001 inch, a = 0.0055 inch). The instability was severe enough to prevent safe operation. Further investigation of this phenomenon at P_s = 150 and zero RPM showed that air hammer persisted up to loads of 4.5 lbs. per bearing and at higher loads it disappeared. When unstable, vibrations occurred in linewith load only (vertical plane) at a frequency of 249 cps and were sinusoidal in form. At 200 psia vibrations persisted up to bearing loads of 12 lbs. per bearing, again sinusoidal, and in the vertical plane only at a frequency of 269 cps.

Pneumatic hammer investigation was not included in the scope of this program; however, pneumatic hammer appears to be a function of bearing geometry, supply pressure and bearing load. The frequency of oscillation seems to be unaffected by load, and affected by supply pressure only for a constant bearing geometry.

3. Fractional-Frequency Whirl

The results obtained in this series of tests on onset of fractional frequency whirl are presented in figures 4 - 9. Figures 4 - 6 show the effect of orifice size on onset of fractional-frequency whirl at various pressures keeping all other factors constant. The variation in orifice size is accomplished through orifice insert change only, leaving the 0.052 inch diameter bearing orifices in the system. This results in inherent rather than orifice compensation and, as such, has to be taken into consideration when analysis is made for comparison with test data. For the conditions represented in figure 4, the orifice size appears to have little or no effect on the onset of fractional-frequency whirl. This is due to the fact that the major restriction with the tight clearance is formed not by the area of the orifice incorporated in the insert, but by the annular area of the permanent set of 0.052 inch diameter orifices in the bearings, or combinations of both restrictors in series. It is also interesting to note that in every instance the onset of fractional-frequency whirl at zero supply pressure occurred at a higher speed than at 50 psia supply pressure. This clearly indicates that in many externally pressurized gas bearing applications, the hydrodynamic effects are significant, and must be included in stability analysis.

Results given in figures 4 - 6 are replotted in figures 7 - 9 as functions of clearance. At low supply pressure, where the hydrodynamic effects predominate, the onset of fractional-frequency whirl increases with increase in clearance. This should not be generalized since the authors in their past work (Ref. 7, page 18) have shown that a clearance exists for each bearing geometry which will produce the onset of instability at lowest speed. Either an increase or decrease in clearance from this

value will produce an increase in threshold of instability. Orifices in the bearing can also significantly influence the threshold of instability. The hydrodynamic effects for the low and high supply pressure conditions are shown in figure 10. Each graduation on the CRO screen represents 0.0001 inch, and the center of the screen represents bearing center. The shaft center is represented by the whirl paths. As can be seen with the bearing geometry indicated, when externally pressurized with 50 psia, the shaft rests on the bearing, and not enough load carrying capacity is available to lift the 6.57 lbs. per bearing load. As soon as shaft begins to spin, however, the shaft center follows a hydrodynamic path. On the other hand, with pressures of 100 psia and above, the position of the shaft when rotating does not differ appreciably from its static position. The whirl amplitudes at speeds below the lowest critical are caused by slight amounts of unbalance. The whirl amplitudes at higher speeds accompanied by phase changes indicate that the rotor is going through critical. This is shown more clearly in figure 11 where pictures show the rotor unit went through both criticals. The photo taken at the highest speed indicates onset of fractional frequency whirl. The frequencies of rotor oscillation at this onset could not be determined since in most cases the onset was quick and violent. Efforts to determine the onset of instability at high speed and high supply pressure conditions resulted in three bearing seizures.

4. Effects of Load on Onset of Fractional-Frequency Whirl

The evaluation of effects of load on onset of fractional-frequency whirl had to be limited to a few points due to the fact that onset was violent

and destructive. Again, as in the other tests, a dependence upon the relative influence of hydrodynamic and hydrostatic effects can be seen in figure 12. At low pressure conditions where the hydrodynamic effects are predominant, the effect of increasing load is to increase the speed at which fractional-frequency whirl occurs. At high pressure, however, this effect becomes modified due to the increase in the load carrying capacity of the bearing. Figure 13 represents effects of load on onset of fractional-frequency whirl at constant pressures of 50 psia as a function of orifice size. Again at these low pressures, hydrodynamic effects predominate and one cannot expect to obtain appreciable benefits from a change in the size of the feeding restrictor.

5. Load Carrying Capacity

Results on load carrying capacity tests are presented in figures 14 - 21 where the test data is superimposed on analytical results. Correlation between theory and test results is good for radial clearances of 0.001 inch and 0.0015 inch up to eccentricity ratios of roughly 0.5. Above those ratios the slope of the load vs. displacement curves seems to be decreasing for the 0.001 inch radial clearance, the decrease being more pronounced at lower pressures. For the 0.0015 inch clearance at pressures of 100 psi and above, the slope seems to be increasing at higher eccentricities over a considerable displacement range and decreasing again as the eccentricity approaches the radial clearance. The reasons for this are not apparent at this time. Considerable disagreement between theory and test data appears in the tests involving 0.0005 inch radial clearance. This can be explained by the fact that the coefficient of discharge for the bearing in theoretical analysis was matched for one clearance (c=0.001 inch)

and thereafter used for all clearance theoretically calculated.

6. Flow Measurements

Results of flow measurements for all conditions are given in figures 22 - 24. As expected, the flow is dependent upon pressure, clearance and orifice size. The effects of inherent compensation are clearly shown in figures 22 and 23 where changes from $a = 0.010$ inch to $a = 0.015$ inch do not result in appreciable flow changes. Excellent agreement between theory (as indicated by dotted lines) and experiment is indicated for radial clearances of 0.0005 and 0.001 inch. Appreciable discrepancies reaching a maximum of 80% at the highest pressure (200 psia) are indicated for the radial clearance of 0.0015 inch. This again can be explained by the fact that the discharge coefficient in the theoretical analysis was matched for the clearance of 0.001 inch and used for all other clearances.

The effects of rotor speed on flow are shown in figures 25 and 26. The decrease in flow with speed is more pronounced at higher pressure levels than at the lower levels.

The relative comparison between discrepancies in flow and load carrying capacity results show that in both cases good agreement exists at the clearance value of 0.001 inch as expected since the discharge coefficient was matched for this particular clearance. At the minimum and maximum clearance, however, the discrepancies between experiment and theory are most pronounced for the load carrying capacity at clearances of 0.0005 inch and for flow at 0.0015 inch. This observation warrants a closer scrutiny of the variation of discharge coefficient as a function of change in feeder parameter and clearance.

IV. THEORETICAL ANALYSIS

The theoretical calculations are concerned with the load carrying capacity and the gas flow for the purely hydrostatic bearing. The onset of instability due to rotation will not be analyzed. The present theoretical results are based on the analysis presented in Reference 10. However, this analysis is limited to orifice restricted bearings and does not take into account the additional flow restriction caused by "inherent compensation" (i.e., the restriction due to the annular area between the rim of the feeding hole and the surface of the journal). For the present test bearing, the feeding hole diameter is sufficiently small to make this effect very important, even being dominant for the tests with the largest orifice size. Thus, it is necessary to incorporate the inherent compensation in the analysis of Reference 10. The journal bearing is pressure-fed from orifice restricted feeding holes on the circumference in the centerplane of the bearing. For a sufficiently large number of feeding holes, these may be approximated by a line source such that the gas feeding becomes a boundary condition to the differential equation describing the flow in the bearing. The differential equation is Reynolds equation which for a perfect gas under isothermal conditions may be written:

$$\frac{\partial}{\partial \bar{X}}\left[\bar{P}\bar{h}^3 \frac{\partial \bar{P}}{\partial \bar{X}}\right] + \frac{\partial}{\partial \bar{Z}}\left[\bar{P}\bar{h}^3 \frac{\partial \bar{P}}{\partial \bar{Z}}\right] = 0 \qquad (1)$$

($\bar{P}$ = pressure, psia - $\bar{h}$ = film thickness, inch - x = circumferential coordinate, inch = z = axial coordinate, inch).

To make dimensionless set:

$$\theta = \frac{X}{R} \qquad \zeta = \frac{Z}{R} \qquad P = \frac{\bar{P}}{P_a} \qquad h = \frac{\bar{h}}{C} = 1 + \varepsilon\cos\theta$$

(R = bearing radius, inch - C = radial bearing clearance, inch - P_a = ambient pressure, psia - $\bar{\varepsilon}$ = eccentricity ratio).

Then:

$$\frac{\partial}{\partial \theta}\left[Ph^3 \frac{\partial P}{\partial \theta}\right] + \frac{\partial}{\partial \zeta}\left[Ph^3 \frac{\partial P}{\partial \zeta}\right] = 0 \qquad (2)$$

Writing the pressure as a power series of the eccentricity ratio ϵ :

$$P = P_0 + \epsilon P_1 + \epsilon^2 P_2 + \text{----} \tag{3}$$

and substituting back into Eq. (2) yields:

$$P_0^2 = 1 + p^2(\xi - \xi) \tag{4}$$

$$\frac{\partial^2(P_0 P_1)}{\partial \theta^2} + \frac{\partial^2(P_0 P_1)}{\partial \xi^2} = 0 \tag{5}$$

(ξ = L/D - L = bearing length, inch - D = bearing diameter, inch - p = feeding constant, to be determined later).

Terms of higher order than the first shall be neglected, i.e., we assume that is small.

In the center of the bearing (ξ = 0) the mass flow through the feeding holes are set equal to the flow leaving through the bearing.

It shall be assumed that the flow through the feeding holes may be considered as a flow through two orifices in series with the same orifice coefficient, but with different flow area. Then the exact mass flow equation is:

$$\frac{M}{A_1 \frac{\eta \sqrt{\frac{2K}{K-1}}}{\sqrt{RT}} \cdot \bar{P}_s} = \left(\frac{\bar{P}_2}{\bar{P}_s}\right)^{1/K} \sqrt{1 - \left(\frac{\bar{P}_2}{\bar{P}_s}\right)^{\frac{K-1}{K}}} = \frac{1}{\beta}\left(\frac{\bar{P}_2}{\bar{P}_s}\right)\left(\frac{\bar{P}_1}{\bar{P}_2}\right)^{1/K} \sqrt{1 - \left(\frac{\bar{P}_1}{\bar{P}_2}\right)^{\frac{K-1}{K}}} \tag{6}$$

(M = mass flow, lbs. sec/in. - $\bar{R}$ = gas constant, in.^{2}/sec.$^2{}^\circ$R - T = absolute temperature, $^\circ$R - η = adiabatic orifice coefficient - K = adiabatic exponent - $\bar{P}_s$ = supply pressure, psia - $\bar{P}_1$ = downstream pressure after second orifice, psia - $\bar{P}_2$ = pressure between first and second orifice, psia - A_1 = area of first orifice, in.^{2} - β = area ratio between first and second orifice). In Eq. (6) the pressure ratio (P_2/P_s) and (P_1/P_2) cannot exceed the critical pressure ratio $(2/k+1)^{k/k-1}$.

To remove this discontinuity Eq. (6) shall be replaced by an approximate expression:

$$M = \frac{\alpha A_1 \bar{P}_s}{\sqrt{\bar{R}T} \cdot \sqrt{1+\beta^2}} \cdot \sqrt{1 - \left(\frac{\bar{P}_1}{\bar{P}_s}\right)^2} \tag{7}$$

(α = orifice coefficient).

A graphical comparison between Eq. (6) and (7) based on K = 1.4 shows that $\alpha = .78 \cdot \sqrt{\eta}$; setting $\eta = .95$ gives $\alpha = .71$ which value has been used in the present calculations. The flow per inch circumference from the feeding holes is $\frac{NM}{2\pi R}$ (N = number of feeding holes). Equating this to the flow per inch into the bearing: $-2\frac{\bar{h}^3}{12\mu}\frac{\bar{P}_i}{\bar{R}\bar{T}}\left(\frac{\partial \bar{P}}{\partial Z}\right)_i$ gives: $\left(\frac{\partial P^2}{\partial \xi}\right) = -\Lambda_t\left[1 - \frac{3+2\sigma^2}{1+\sigma^2}\cos\theta\right]\sqrt{V^2 - P_i^2}$

(8)

where:

$$\Lambda_t = \frac{6\mu N a^2 \alpha}{P_a C^3} \cdot \sqrt{\frac{\bar{R}T}{1+\sigma^2}} \qquad (9)$$

(μ = viscosity, lbs.sec/in^2 - a = orifice radius, inch - $V = P_s/P_a$, pressure ratio - $\sigma = a^2/dC$, orifice area ratio - d = diameter of feeding hole, inch).

Using Eq. (8) as a boundary condition to Eq. (4) and (5) and proceeding as in Ref. 10 we obtain the bearings load carrying capacity and flow:

$$W = \frac{1+\frac{3}{2}\sigma^2}{1+\sigma^2} \cdot \frac{\pi}{4} D L^2 \xi \frac{3}{u}\left\{\frac{e^{-u^2}\left[\psi\left(\sqrt{u^2+\xi}\right) - \psi(u)\right] - \frac{\sqrt{\pi}}{2}e^{u^2}\left[\varphi\left(\sqrt{u^2+\xi}\right) - \varphi(u)\right]}{\xi\left[\cosh\xi + \Lambda_t^2 u^2 \sinh\xi\right]}\right\} \text{lbs} \qquad (10)$$

$$Q = \frac{\pi C^3 P_a^2}{6\mu\bar{R}T} \cdot \frac{1}{u^2} \quad \frac{\text{lbs}\cdot\text{sec}}{\text{in}} \qquad (11)$$

where:

$$u = \frac{1}{\gamma} = \left[\frac{\xi\Lambda_t^2}{2}\left(-1 + \sqrt{1 + \frac{4(V^2-1)}{\xi^2\Lambda_t^2}}\right)\right]^{-1/2}$$

$$\psi(x) = \int_0^x e^{t^2} dt \qquad \varphi(x) = \operatorname{erf}(x) = \frac{2}{\sqrt{\pi}}\int_0^x e^{-t^2} dt$$

Except for the factor $\frac{1+\frac{3}{2}\sigma^2}{1+\sigma^2}$ in Eq. (10) and the modification of Λ_t these two equations are identical with the results obtained in Ref. 10.

From Eqs. (9), (10), and (11) numerical results are obtained for the load carrying capacity and the flow. The results are plotted together with the experimental data

in figures 14 - 24. The calculations are based on the following data:

Bearing length-to-diameter ratio $\xi = \frac{1}{2}$

Bearing radius R = 1 inch

Radial clearance C = .0005 inch - .001 inch - .0015 inch

Diameter of feeding hole: d = .052 inch

Number of feeding holes: N = 8

Orifice coefficient α = .71

Orifice radius a = .0055 inch - .010 inch - .015 inch

Ambient pressure P_a = 14.7 psia

Supply pressure P_s = 50 psia - 100 psia - 150 psia - 200 psia

Gas viscosity μ = 2.828×10^{-9} lbs.sec/in.^{2} (air at 70°F)

Gas constant x Total temperature $\bar{R}$ T = 339,300 lbs.in/lbs. (air at 70°F)

Whirl Analysis

If one accepts the model of a constant speed whirl motion centering around the axis of the bearing such that the orbit of the shaft center is a circle, then it has been shown rigorously, for an isothermal gas film, that the effective bearing number is (Refs. 1, 2, 3):

$$\Lambda^* = \Lambda \left(1 - \frac{2\dot{\phi}}{\omega}\right) ;$$

where $$\Lambda = \frac{6\mu\omega}{P_a} \left(\frac{R}{C}\right)^2$$

More specifically, with the approximations of small Λ^* and e/C the hydrodynamic film forces during a steady translatory whirl motion are:

$$F_{rh} = K_2 (\omega - 2\dot{\phi})^2 e ;$$
$$F_{th} = K_1 (\omega - 2\dot{\phi}) e ; \qquad (12)$$

where K_1 and K_2 are functions of Λ and L/D, and have the dimensions of the product of the stiffness and the first and second powers of time respectively. Using these relations, following an analysis otherwise similar to reference 4, the conditions for neutral stability (self-sustained whirl motion) are:

$$\frac{\Omega}{\omega_o} = \frac{1}{\sqrt{1 - \omega_o^2 (\tau_1 - \tau_2)^2 \frac{k_s K_2}{(K_1)^2}}} \quad ; \tag{13}$$

$$\frac{\omega}{\Omega} = 2 + (\tau_1 - \tau_2) \frac{k_s}{K_1} \tag{14}$$

where

Ω = whirl speed,

ω = shaft speed at neutral stability,

τ_1, τ_2 = lead and lag time constants of pressurization system.

$$\omega_o = \sqrt{\frac{2 k_s}{m}}$$

Above results also employed the assumption

$$\tau_2^2 \ \Omega^2 << 1$$

The above result can be rearranged as

$$\lambda = \frac{\omega}{\Omega} - 2 = (\tau_1 - \tau_2) \frac{k_s}{K_1} \quad ; \tag{15}$$

$$\frac{\Omega}{\omega_o} = \frac{1}{\sqrt{1 - \frac{2K_2}{m} \lambda^2}} \tag{16}$$

which reveals the interesting conclusion that the self-sustained whirl can be suppressed if

$$\frac{2K_2}{m} \geq \frac{1}{\lambda^2}$$

V. CONCLUSIONS

1. Good agreement on load carrying capacity and flow for certain clearance values was noted. The disagreements between test and theoretical results for other clearances can be attributed to the assumption of constant coefficient of discharge in calculations which was matched for one particular clearance, but could have been matched for other clearances.
2. Based on load carrying capacity solutions, good agreement between calculated and observed system criticals was obtained.
3. Onsets of fractional-frequency whirl are a function of bearing geometry, load, speed and supply pressure.
4. Hybrid bearings, depending upon supply pressure level and bearing geometry, can be subject to hydrodynamic forces which will have a net effect of producing destructive self-sustained whirl at speeds lower than that of onset of half-frequency whirl, if the bearings had been purely self acting (see figures 4-9)
5. Effects of increase in load on onset of fractional-frequency whirl are pronounced at low supply pressures when self acting effects predominate; same, however, become negligible when supply pressures are raised to the point where static load carrying capacity of the hydrostatic bearing does not result in significant eccentricity at the higher pressures and given load.
6. Air flow in hybrid bearings decreases as speed increases.
7. Theoretical analysis indicates that whirl ratio is a function of lead and lag time constants and the ratio of hydrostatic gas film stiffness to the tangential hydrodynamic gas film stiffness. The whirl ratio can be larger or smaller than 2 depending on the sign of the difference between lead and lag time constants. When hydrostatic effects become negligible, the ratio approaches a limit of 2.
8. Theoretical calculations indicate that onset of FFW can be suppressed if $2\ K_2/m \geq \frac{\Omega}{\omega_1}$

VI. REFERENCES

1. "Static and Dynamic Characteristics of Compensated Gas Bearings", H. Richardson, ASME Paper No. 57-A-138, January 10, 1958.

2. "The Performance of Externally Pressurized Bearings Using Simple Orifice Restrictors", D.S. Allen, P.T. Stokes, S. Whitley, UKAEA, Capenhurst, England, ASLE Preprint No. 60LC-17, Boston, October 17-19, 1960.

3. "Analysis and Design of Externally Pressurized Gas Bearings", I.C. Tang, W.A. Gross, IBM, San Jose, California, ASLE Preprint No. 61LC-20, Chicago, October 17-19, 1961.

4. "Theory of Hydrodynamic Lubrication", O. Pinkus and B. Sternlicht, McGraw-Hill Publication, May, 1961.

5. "On the Hybrid Gas Lubricated Journal Bearing", J. Lund, ONR Contract, February, 1962.

6. "On the Load Capacity and Stability of Rotors in Cylindrical Gas-Dynamic Journal Bearings", B. Sternlicht, L.W. Winn, ONR Report, Contract No. 2844(00), Task No. 097-348, July 3, 1961.

7. "Geometry Effects on the Threshold of Half-Frequency Whirl in Gas Dynamic Journal Bearings", B. Sternlicht, L.W. Winn, ONR Report, Contract No. 2844(00), Task No. 097-348, October 16, 1961.

8. "Some Instabilities and Operating Characteristics of High Speed Gas Lubricated Journal Bearings", G.K. Fischer, J.L. Cherubin, D.D. Fuller, ASME Publication, 58-A-231, November 30, 1958.

9. "Gas Bearing Stability Study-Vertical Rotor Investigation", R.C. Elwell, R.J. Hooker B. Sternlicht, NONR 2844(00), Task No. 097-348, May 20, 1960.

10. "The Theory of the Externally-Pressurized Bearing with Compressible Lubricant", G. Heinrich, First International Symposium on Gas Lubricated Bearings, ONR/ACR-49.

11. "On the Translatory Whirl Motion of a Vertical Rotor in Plain Cylindrical Gas-Dynamic Journal Bearings", C.H.T. Pan and B. Sternlicht, May 8, 1961, ONR Report, Also ASME Paper No. 61-LUB-4.

12. "Gas-Lubricated Cylindrical Journal Bearings of Finite Length - Part II, Dynamic Loading," B. Sternlicht, September 9, 1960, ONR Report.

13. "A Preliminary Study of Whirl Instability for Pressurized Gas Bearings", R. H. Larson and H.H. Richardson, ASME Paper WC-61-113.

VII. APPENDIX A

Table I - Instabilities

Table II - Comparison of Observed with Calculated Criticals

Table I

Instabilities

L/D = .5, D = 2.00", W = 6.57 lbs/brg.

8 Orifices in Central Plane

*Calculated - all others observed on test

Orifice Dia. IN.	Press. PSIA	ω_c RPM	ω_T RPM	FFW RPM	4/3	5/3
			C = 0.0005"			
0.030	50			12,600		
0.020	80			16,700		
	100	13,400*	17,200*	21,640	1.285*	1.61
	150	22,000*	28,300*	33,000	1.285*	1.50
0.011	50			11,700		
	80			16,300		
	100	16,800*	21,600*	22,500	1.285*	1.34*
	150	25,800*	33,200	33,000	1.285*	1.28*
			C = 0.001"			
0.030	50	7,680	10,200	16,240	1.33	2.12
	80	12,100	16,500	38,640	1.36	3.18
	100	14,300	20,780	54,220	1.45	3.80
	150	16,600	22,000	62,260	1.32	3.75
0.020	50	7,600	10,200	16,280	1.34	2.14
	80	12,000	16,400	35,300	1.36	2.94
	100	13,500	21,200	51,000	1.57	3.78
	150	16,000	22,600	62,300	1.41	3.90
	200	17,000	23,500	70,000	1.38	4.12
0.011	50	8,000	11,600	15,350	1.45	1.92
	80	11,000	16,600	22,000	1.51	2.00
	100	12,600	20,800	40,600	1.65	3.22
	150		Air hammer			
			C = 0.0015"			
0.030	50	6,700	9,500	23,000	1.42	3.43
	80	8,100	11,600	38,500	1.43	4.75
	100	8,900	13,000	55,000	1.46	6.20
	150	10,000	14,400	64,000	1.44	6.40
0.020	50	6,700	9,300	20,600	1.39	3.08
	80	8,100	11,600	35,600	1.43	4.40
	100	8,870	12,400	47,000	1.40	5.30
	150	9,800	14,200	62,000	1.45	6.42
0.011	50	6,000	8,000	17,000	1.33	2.84
	80	7,000	9,030	21,200	1.29	3.03
	100	7,800	11,200	22,400	1.44	2.88
	150	10,100	12,450	25,200	1.235	2.50

TABLE II

Criticals

Comparison of Observed with Calculated Criticals

L/D = .5, D = 2.00" W = 6.57 #/bearing

Orifice Dia. in.	Radial Clearance in.	Press. PSIA	ω_c Obs. RPM	** Calc. RPM	ω_T Obs. Rpm	Theo. Rating RPM	* Calc.RPM
0.030	0.0005	50				14,238	
0.020		100		13,400		28,743	17,200
		150		22,000		37,395	28,300
0.011		50				17,953	
		100		16,800		32,458	21,600
		150		25,800		41,014	33,200
0.030	0.001	50	7,680	9,230	10,200	14,047	11,870
		100	14,300	16,860	20,780	20,120	21,700
		150	16,600	19,150	22,000	23,682	24,600
0.020		50	7,600	9,240	10,200	14,524	11,870
		100	13,500	16,600	21,200	20,455	21,300
		150	16,000	19,700	22,600	24,064	25,300
		200	17,000	22,000	23,500	26,566	28,300
0.011		50	8,000	11,350	11,600	14,911	14,600
		100	12,600	17,800	20,800	20,101	22,900
		150	Air Hammer			23,472	
0.030	0.0015	50	6,700	8,000	9,500	10,600	10,280
		100	8,900	10,900	13,000	13,751	14,000
		150	10,000	12,150	14,400	16,024	15,600
0.020		50	6,700	8,050	9,300	10,418	10,300
		100	8,100	10,000	12,400	13,385	13,600
		150	9,800	11,920	14,200	16,243	15,300
0.011		50	6,000	6,820	8,000	8,699	8,760
		100	7,800	9,620	11,200	10,217	12,370
		150	10,100	11,000	12,450	14,052	14,200

* Calculated from static load carrying capacity curves

** Calculated on basis of $\frac{\omega_T}{\omega_c} = 1.285$

VII. APPENDIX B

List of Figures	Description
Figure 1	Test Rig
Figure 2	Orifice Holder
Figure 3	Thrust Plate Detail
Figures 4 - 9	Results on Onset of FFW
Figures 10 -11	CRO Pictures on Dynamic Behavior of Shaft in Externally Pressurized Bearing
Figure 12	FFW vs. Supply Pressure
Figure 13	FFW vs. Load
Figures 14 - 21	Load vs. Eccentricity Curves
Figures 22 - 24	Flow vs. Supply Pressure
Figures 25 - 26	Effect of Speed on Flow

AAT 10159

GAS BEARING TEST SETUP
FIG. 1

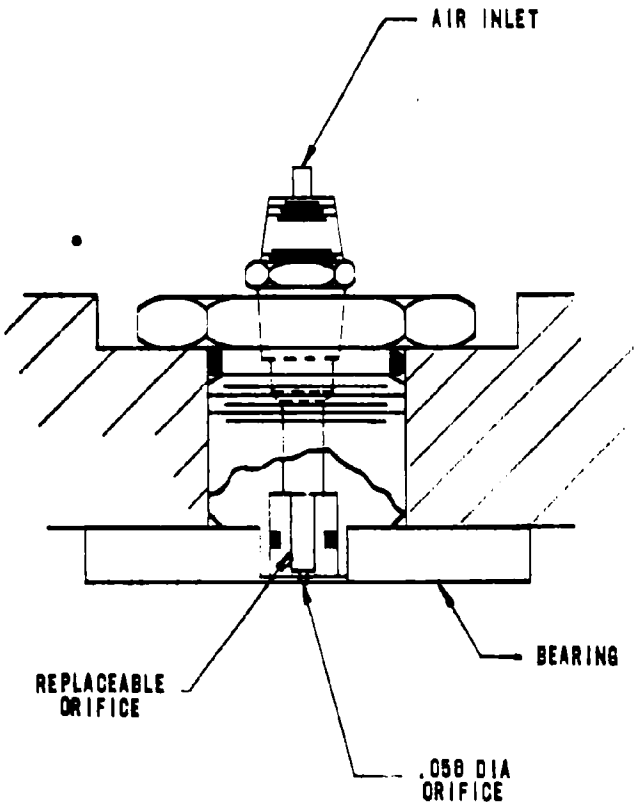

ORIFICE HOLDER
FIG. 2

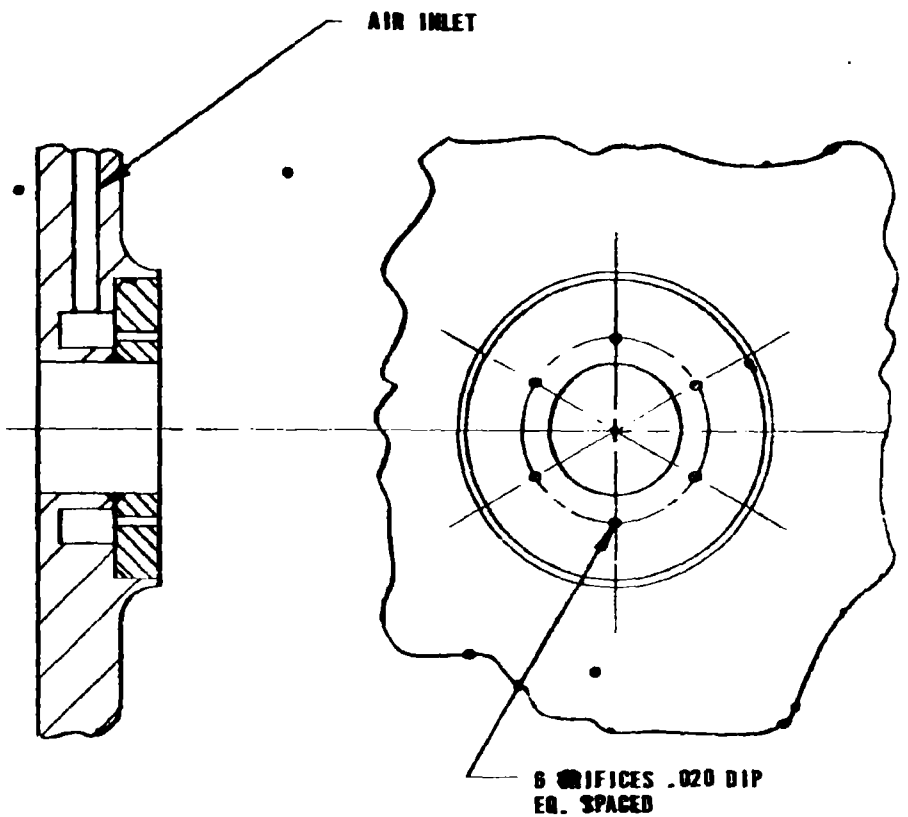

THRUST PLATE
FIG. 3

ONSET OF FRACTIONAL FREQUENCY WHIRL
VS.
SUPPLY PRESSURE
(Effects of clearance)

L/D = .5
D = 2.00"
C = .0005"
⊙-a = .015"
.-a = .010"
△-a = .0055"
W = 6.57 LBS/BRG.

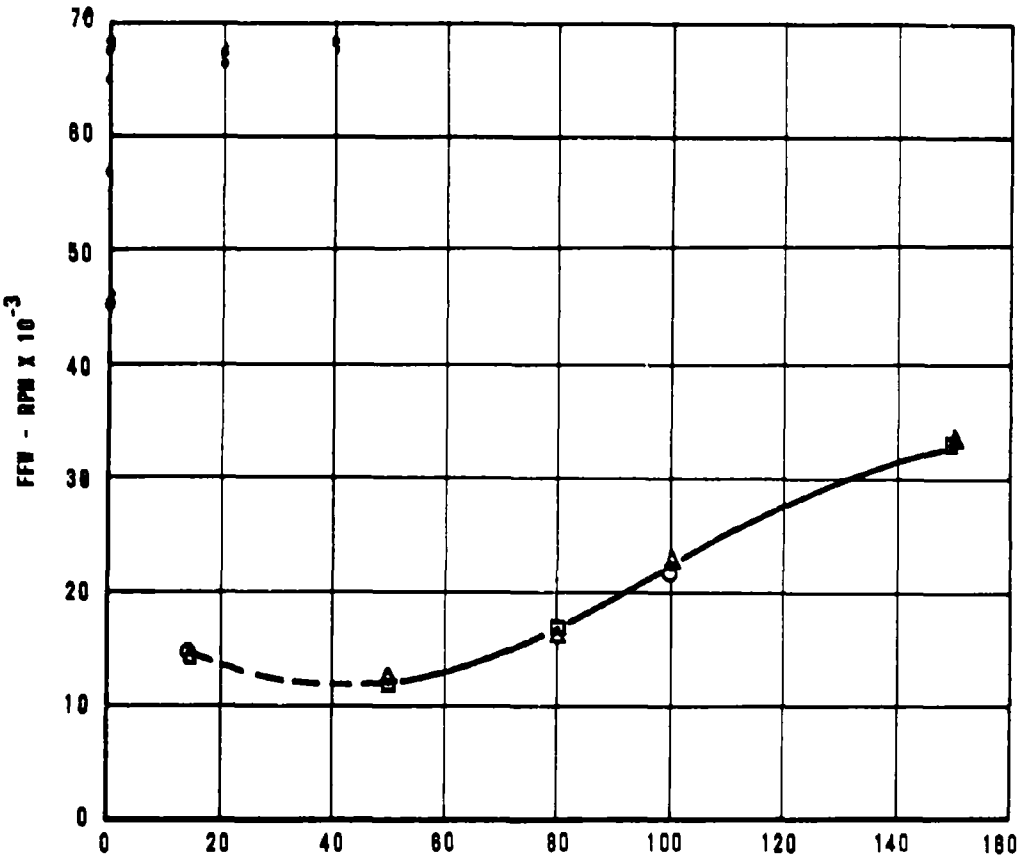

FIG. 4

ONSET OF FRACTIONAL FREQUENCY WHIRL
VS.
SUPPLY PRESSURE
(Effects of orifice size)

L/D = .5
D = 2.00"
C = .001"
⊙-a = .015"
.-a = .010"
△-a = .0055"
W = 8.57 LBS/BRG.

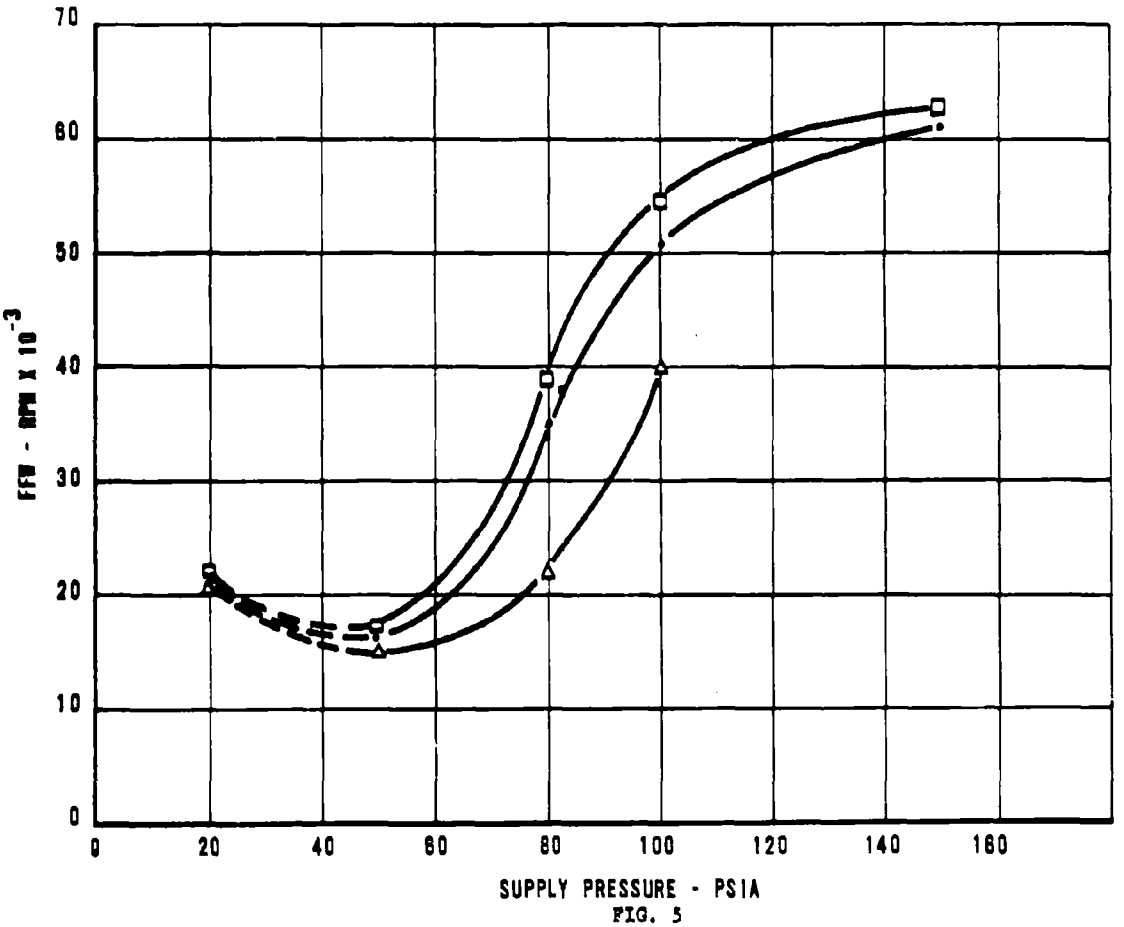

FIG. 5

ONSET OF FRACTIONAL FREQUENCY WHIRL
VS.
SUPPLY PRESSURE
(Effects of orifice size)

L/D = .5
D = 2.00"
C = .0015"
⊙-a = .015"
□-a = .010"
Δ-a = .0055"
W = 6.57 LBS/BRG.

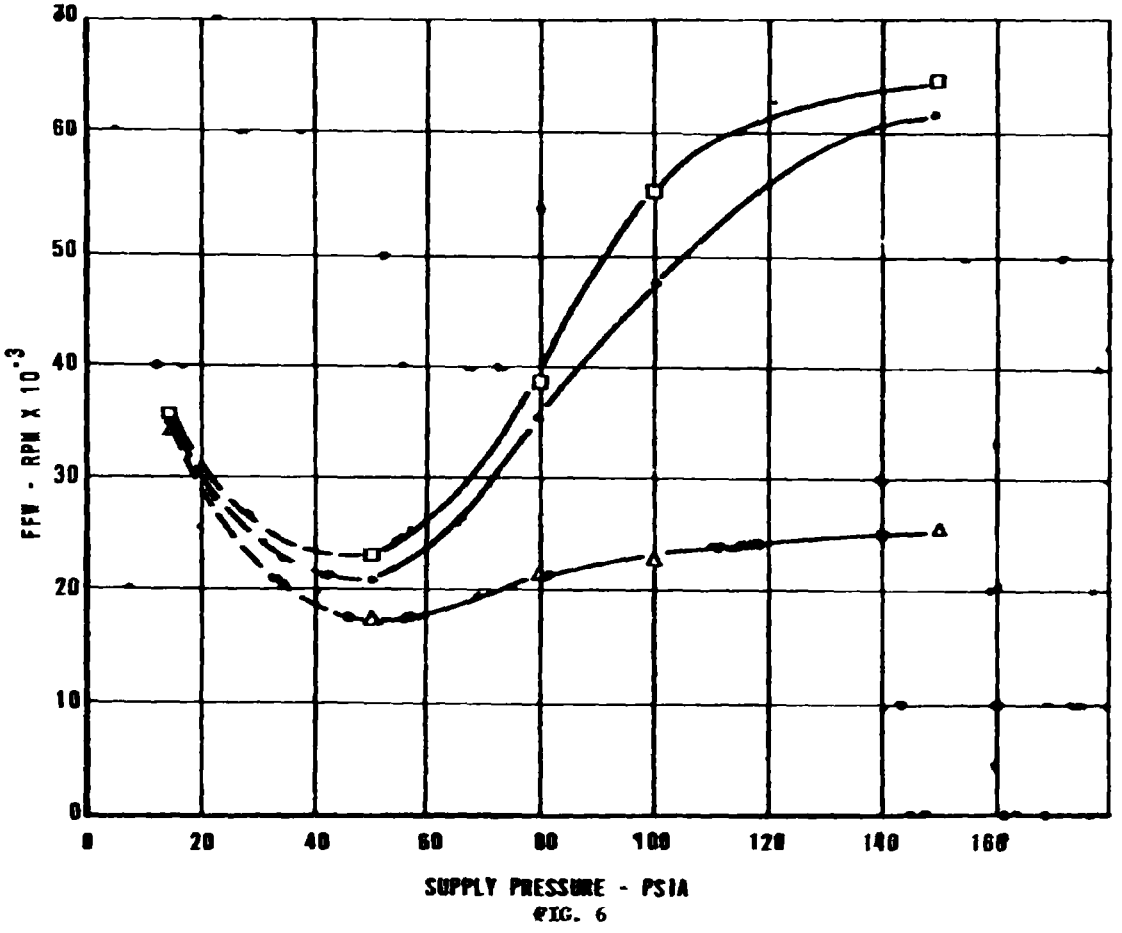

FIG. 6

ONSET OF FRACTIONAL FREQUENCY WHIRL
VS
SUPPLY PRESSURE
(Effects of clearance)

L/D = .5
D = 2.00"
a = .0055"
.-c = .00C5"
□-c = .001"
Δ-c = .0015"
W = 8.57 LBS.

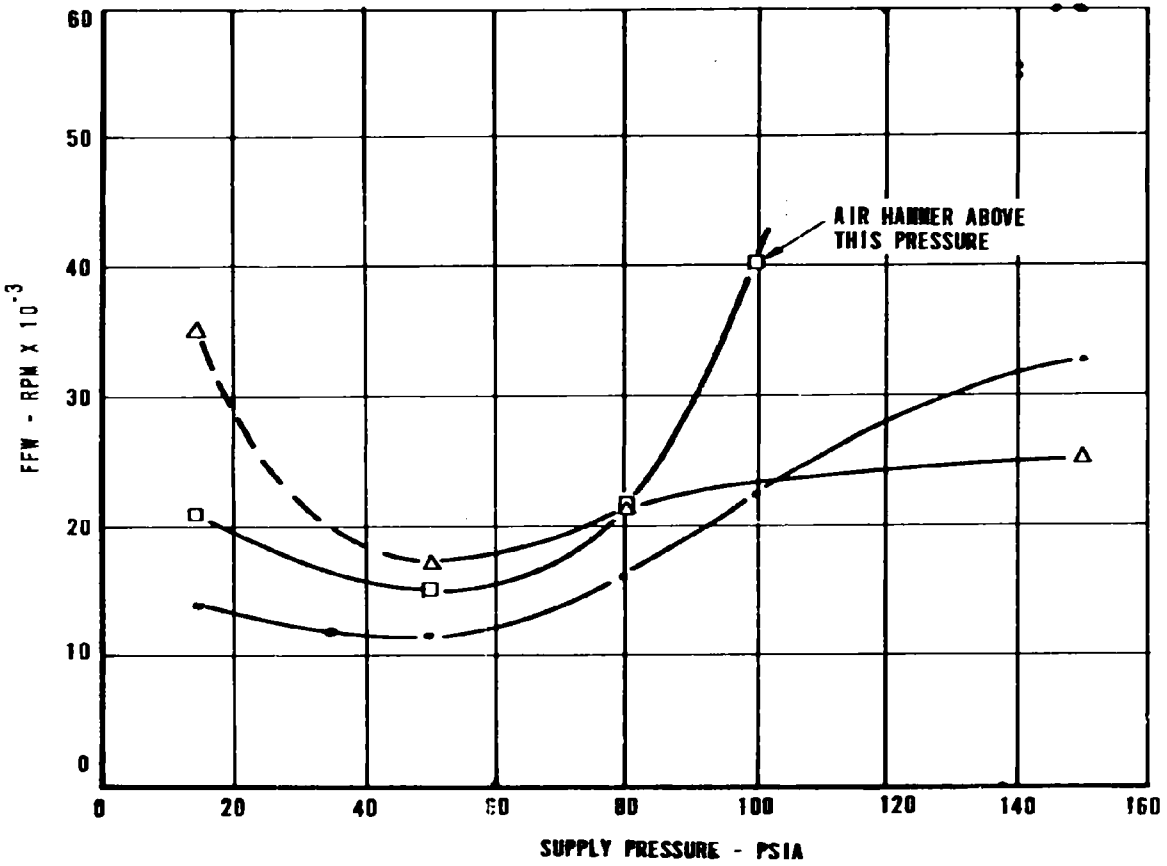

FIG. 7

ONSET OF FRACTIONAL FREQUENCY WHIRL
VS.
SUPPLY PRESSURE
(Effects of clearance)

L/D = .5
D = 2.00"
a = .010"
.-c = .0005"
□-c = .001"
△-c = .0015"
W = 8.57 LBS.

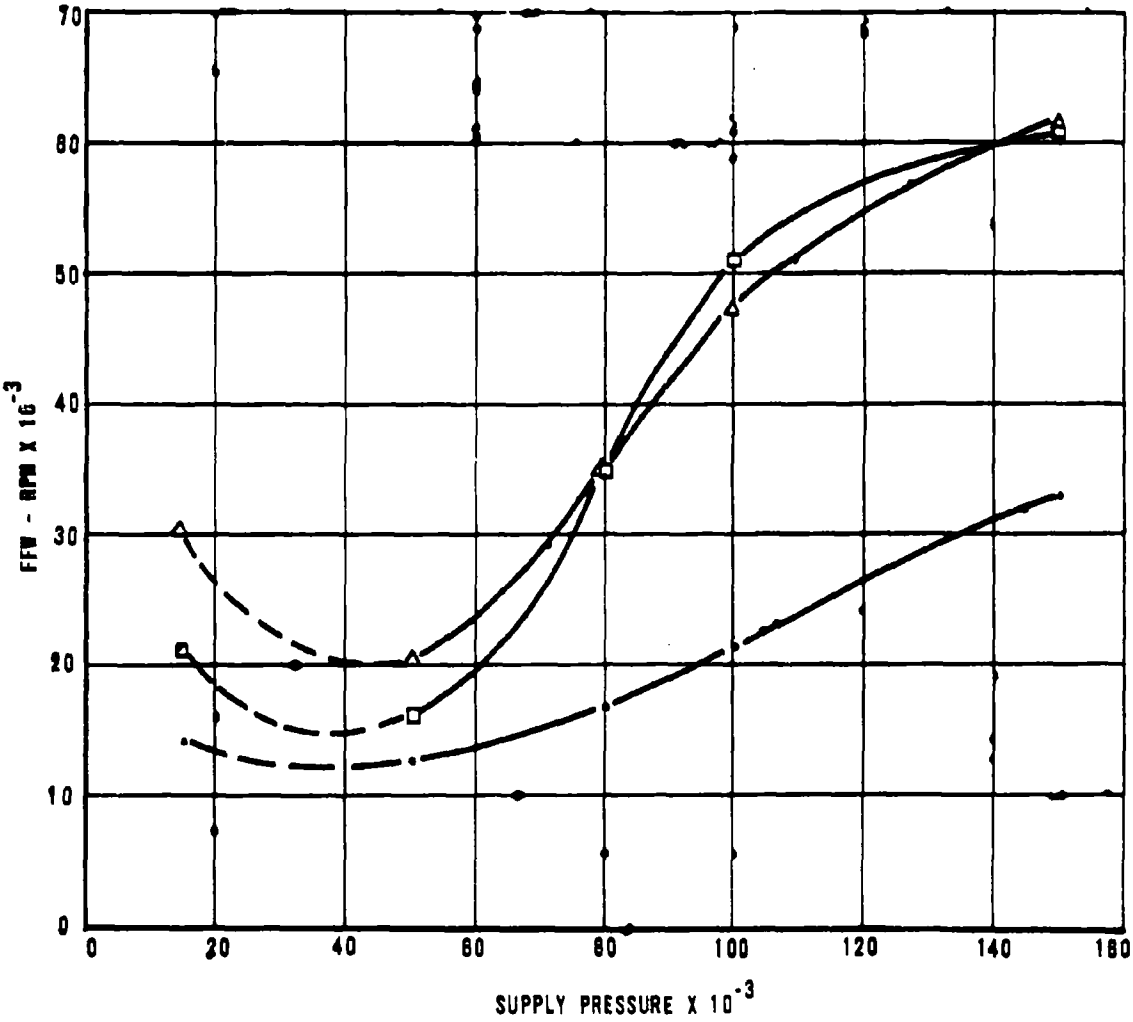

FIG. 8

ONSET OF FRACTIONAL FREQUENCY WHIRL
VS.
SUPPLY PRESSURE
(Effects of clearance)

L/D = .5
D = 2.00"
a = .015"
.-c = .0005"
□-c = .001"
△-c = .0015"
W = 6.57 LBS.

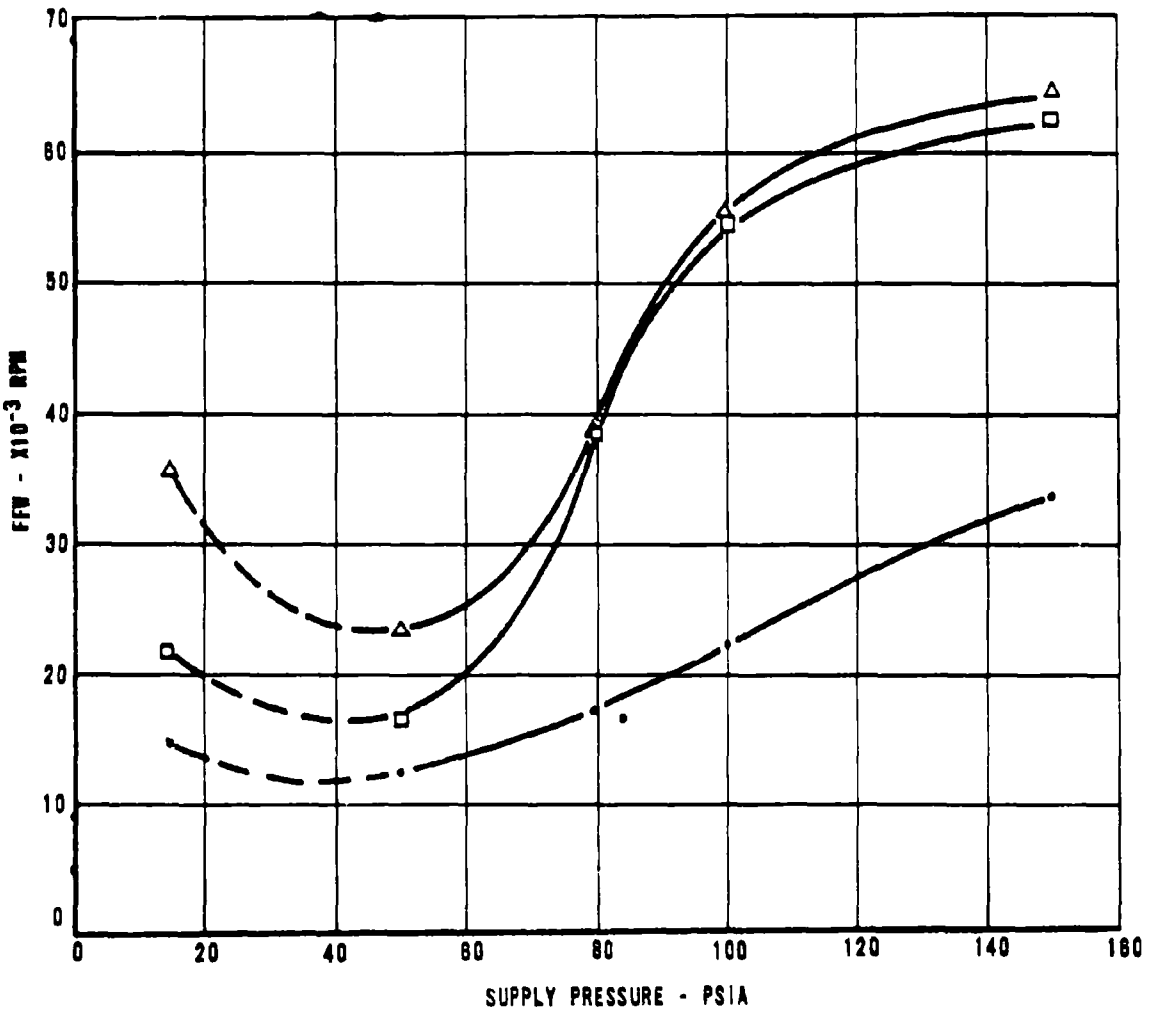

FIG. 9

Dynamic Behavior of Shafts Supported on Externally Pressurized Bearings

Load 6.57 lbs/bearing

c = .0005"

a = .015"

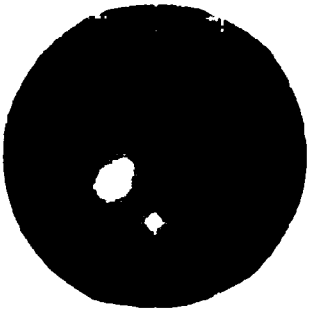

P = 50 psia
Static dot - bottom
2,000 RPM
5,000 RPM
10,000 RPM

P = 100 psia
Static dot - 1 grad.
2,000 RPM
10,000 RPM (large ampl.)
17,000 RPM

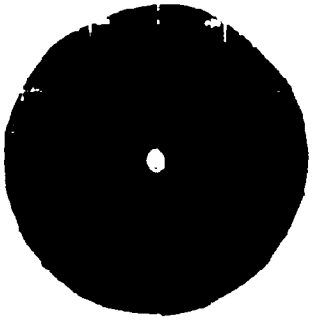

P = 150 psia
Static
10,000 RPM
20,000 RPM (large ampl.)
30,000 RPM

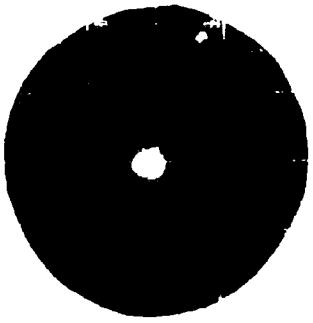

P = 200 psia
Static
10,000 RPM
20,000 RPM (large ampl.)
30,000 RPM

FIG. 10

Dynamic Behavior of Shafts Supported on Externally Pressurized Bearings

Load 6.57 lbs/bearing

c = .001"

a = .015"

P = 50 psia

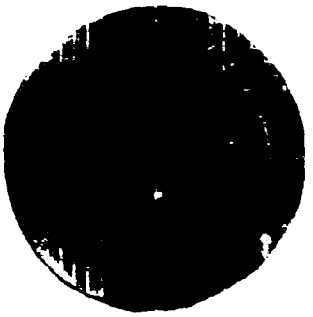

Static

7680 RPM (large ampl.)
8300 RPM

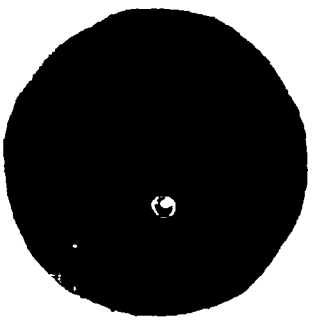

10,000 RPM (large ampl.)
15,000 RPM

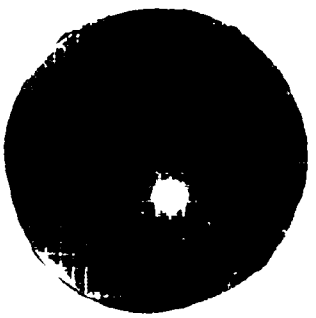

16,246 RPM
onset of whirl

FIG. 11

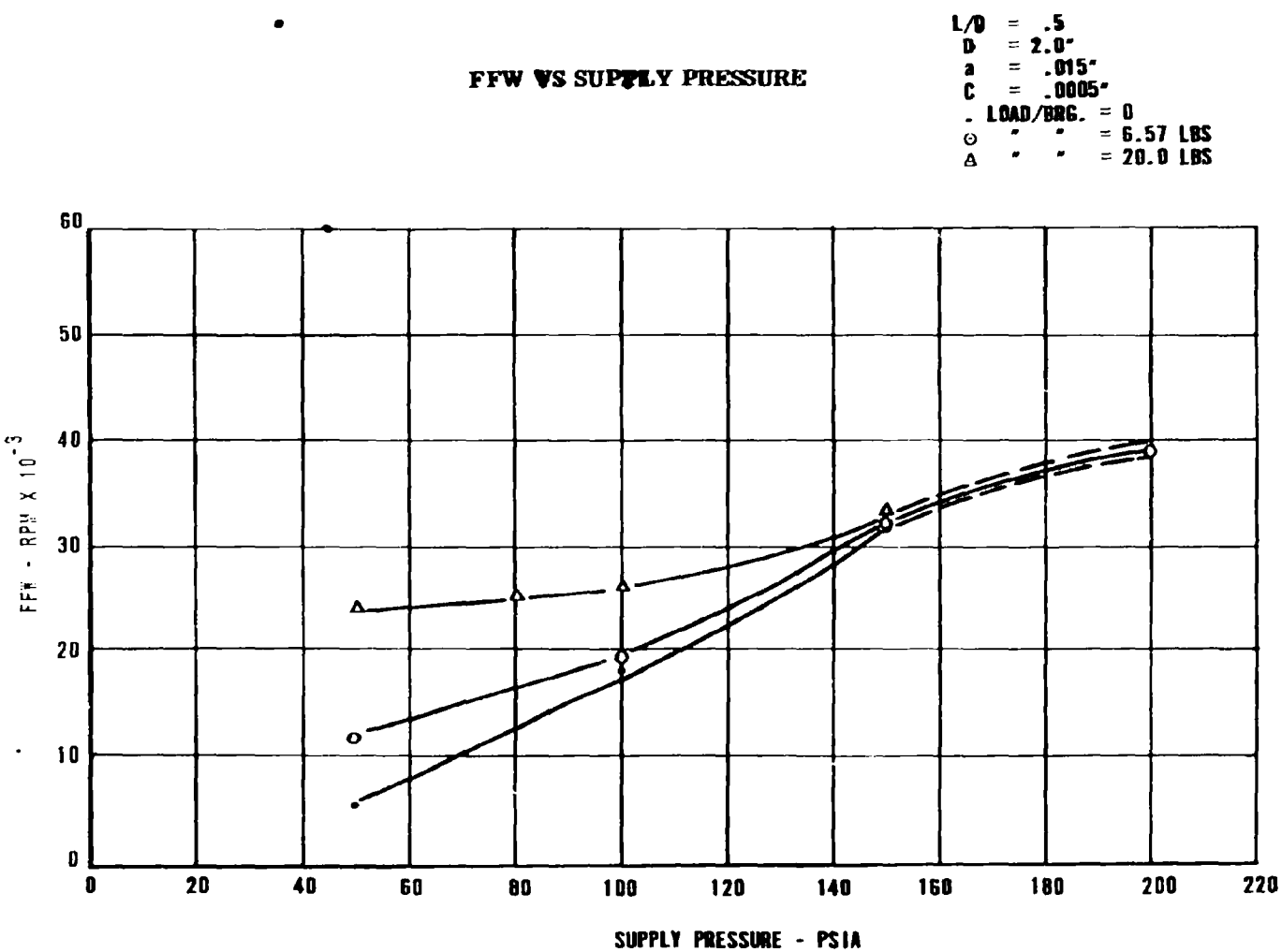
FFW VS SUPPLY PRESSURE
L/D = .5
D = 2.0"
a = .015"
C = .0005"
• LOAD/BRG. = 0
⊙ " " = 6.57 LBS
△ " " = 20.0 LBS
FFW - RPM X 10^-3
0
10
20
30
40
50
60
0
20
40
60
80
100
120
140
160
180
200
220
SUPPLY PRESSURE - PSIA

FIG. 12

FFW VS. LOAD

L/D = .5
D = 2.0"
C = .001"
P_s = 50 PSIA
⊙-e = .015"
.-e = .010"
△-e = .005"

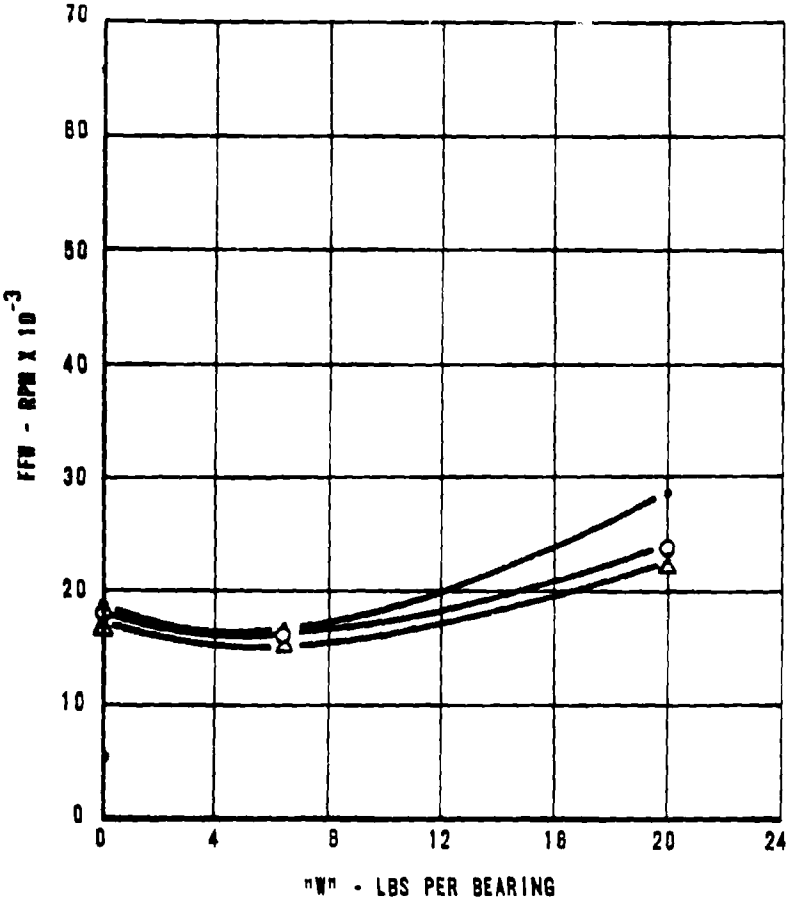

FIG. 13

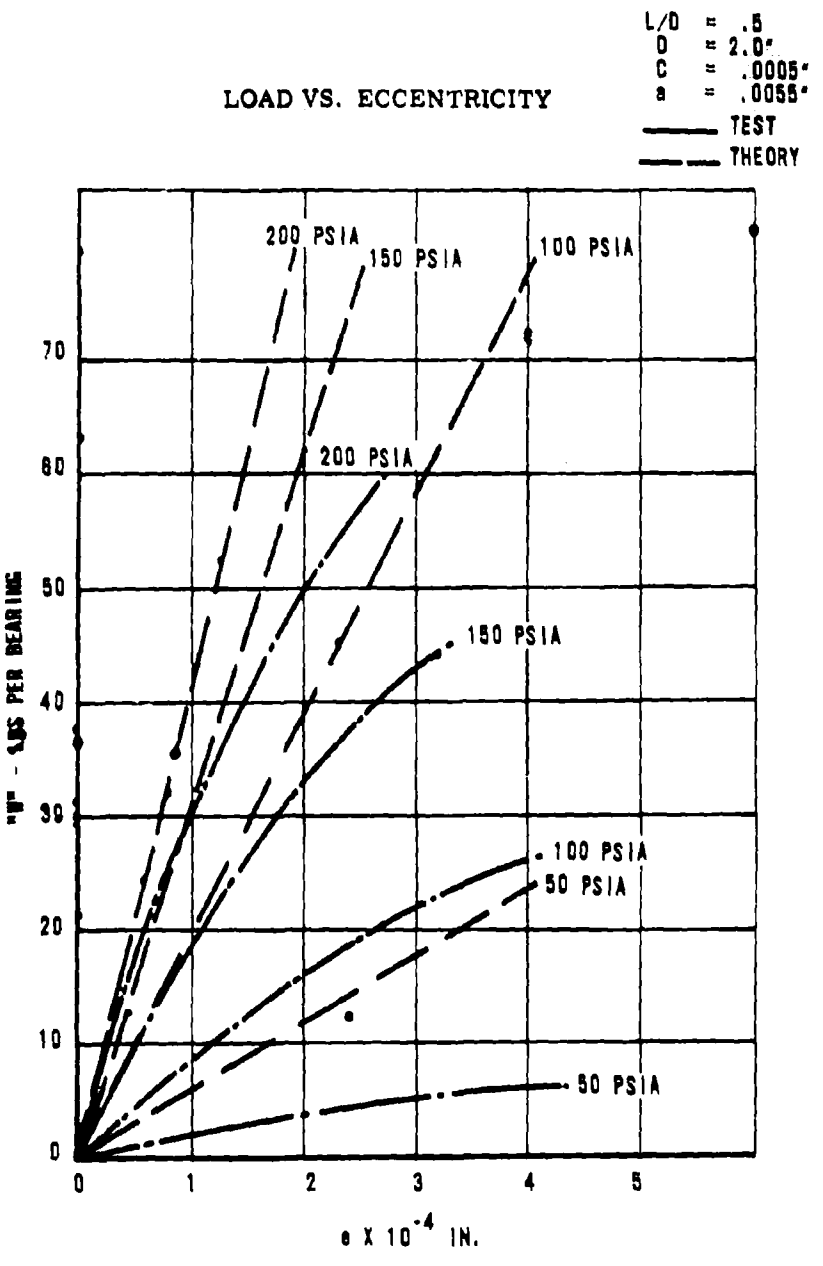
LOAD VS. ECCENTRICITY
L/D = .5
D = 2.0"
C = .0005"
a = .0055"
TEST
THEORY
200 PSIA
150 PSIA
100 PSIA
200 PSIA
150 PSIA
100 PSIA
50 PSIA
50 PSIA
"W" - LBS PER BEARING
0
10
20
30
40
50
60
70
0
1
2
3
4
5
e X 10^-4 IN.

FIG. 14

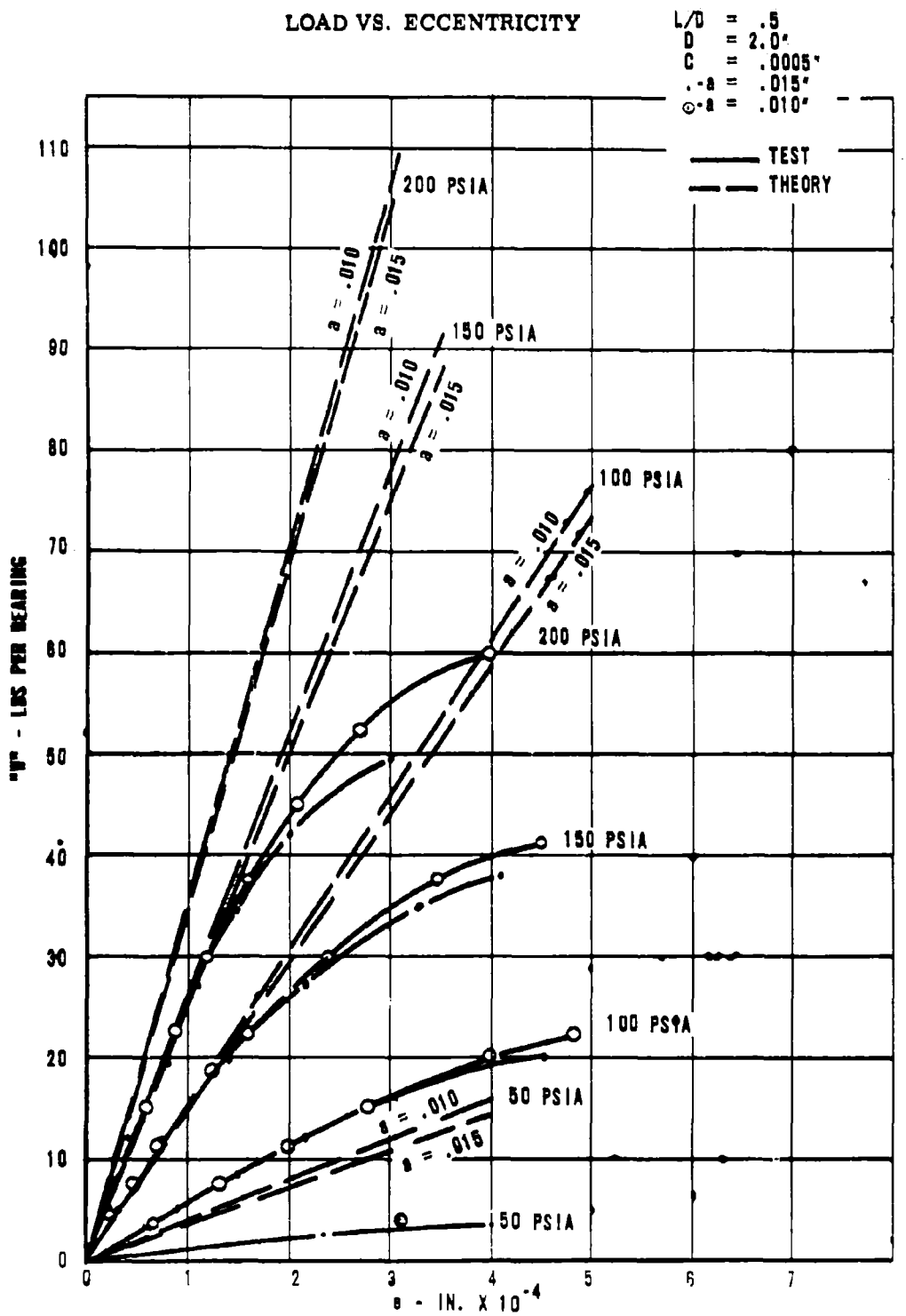
LOAD VS. ECCENTRICITY
L/D = .5
D = 2.0"
C = .0005"
.-a = .015"
⊙-a = .010"
TEST
THEORY
200 PSIA
150 PSIA
100 PSIA
50 PSIA
a = .010
a = .015
"W" - LBS PER BEARING
ε - IN. X 10⁻⁴
0
10
20
30
40
50
60
70
80
90
100
110
1
2
3
4
5
6
7

FIG. 15

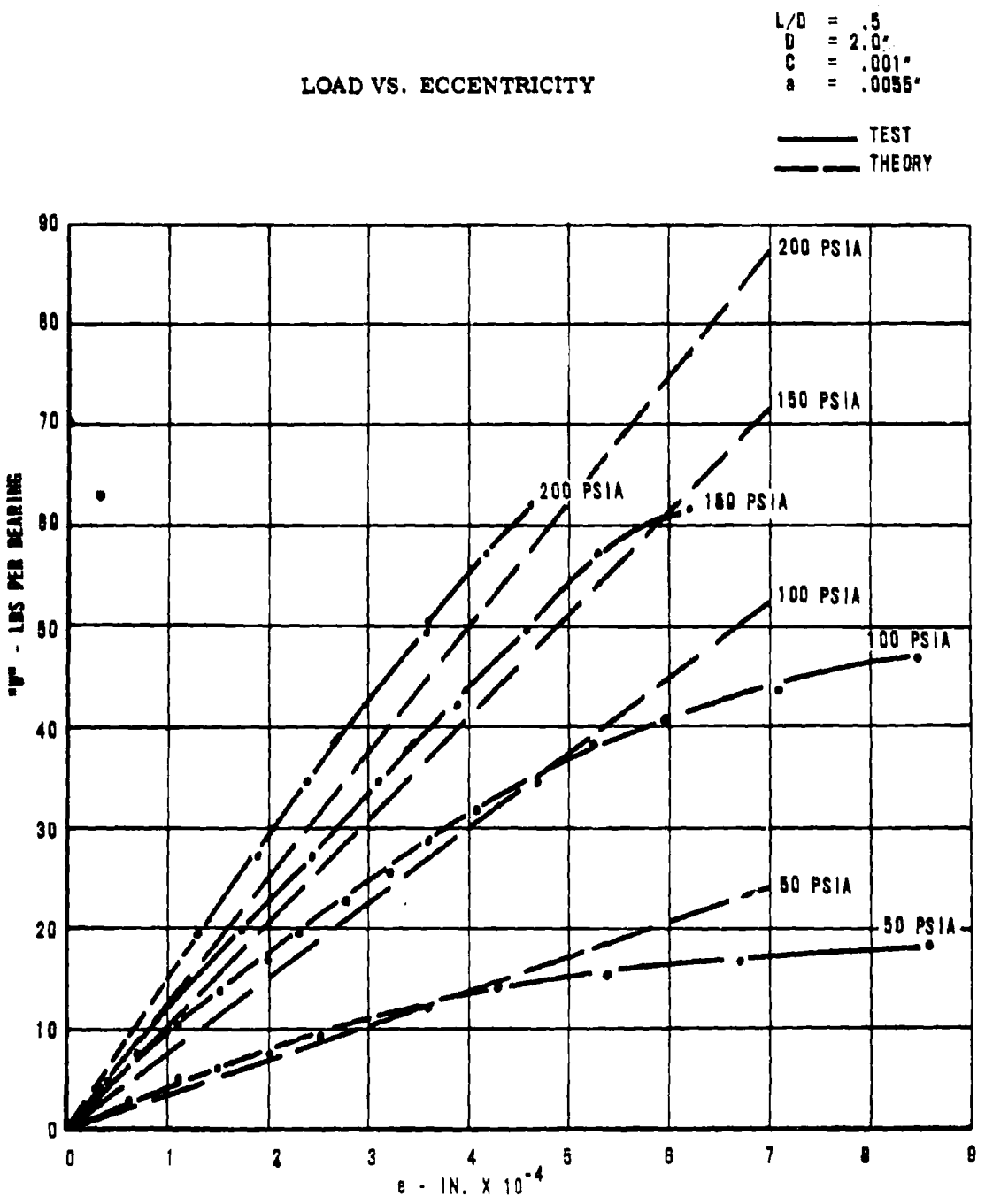
LOAD VS. ECCENTRICITY
L/D = .5
D = 2.0"
C = .001"
a = .0055"
TEST
THEORY
200 PSIA
150 PSIA
200 PSIA
150 PSIA
100 PSIA
100 PSIA
50 PSIA
50 PSIA
"W" - LBS PER BEARING
e - IN. X 10^-4
0
10
20
30
40
50
60
70
80
90
0
1
2
3
4
5
6
7
8
9

FIG. 16

LOAD VS. ECCENTRICITY

L/D = .5
D = 2.0"
C = .001"
a = .010"

——— TEST
— — — THEORY

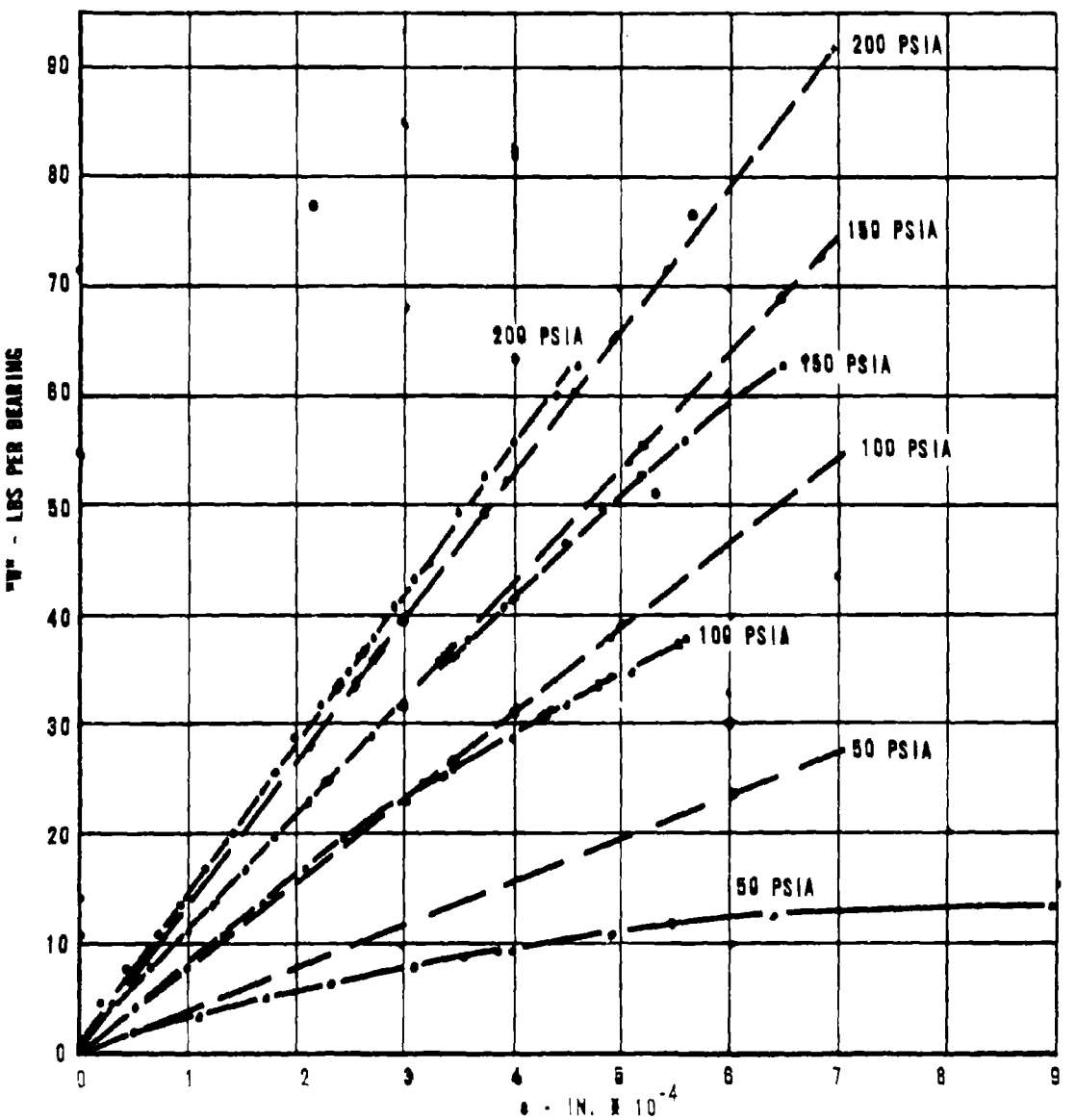

FIG. 17

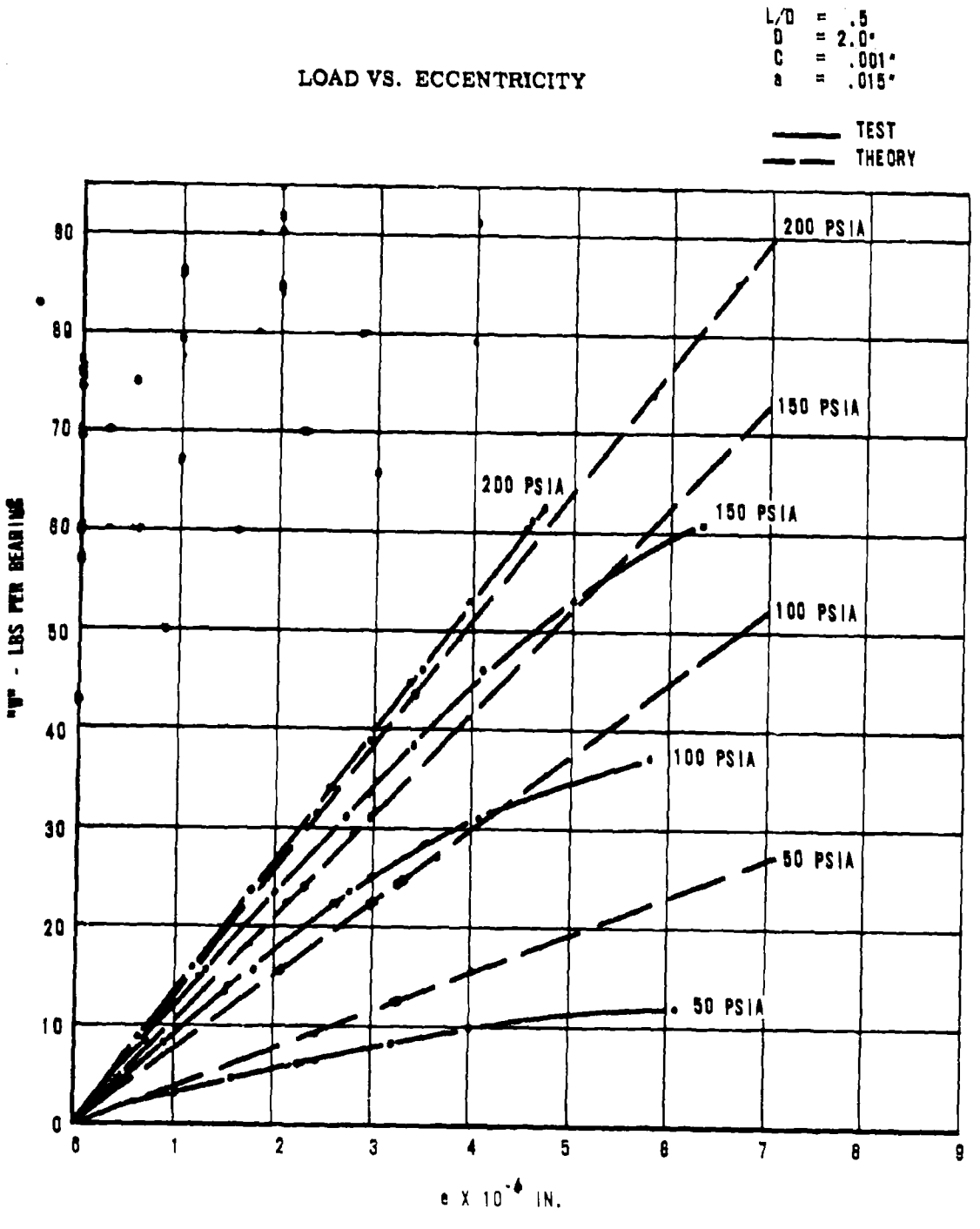
LOAD VS. ECCENTRICITY
L/D = .5
D = 2.0"
C = .001"
a = .015"
TEST
THEORY
200 PSIA
150 PSIA
200 PSIA
150 PSIA
100 PSIA
100 PSIA
50 PSIA
50 PSIA
"W" - LBS PER BEARING
e X 10⁻⁴ IN.
0
10
20
30
40
50
60
70
80
90
0
1
2
3
4
5
6
7
8
9

FIG. 18

LOAD VS. ECCENTRICITY

L/D = .5
D = 2.0"
C = .0015"
ε = .005"

——— TEST
— — — THEORY

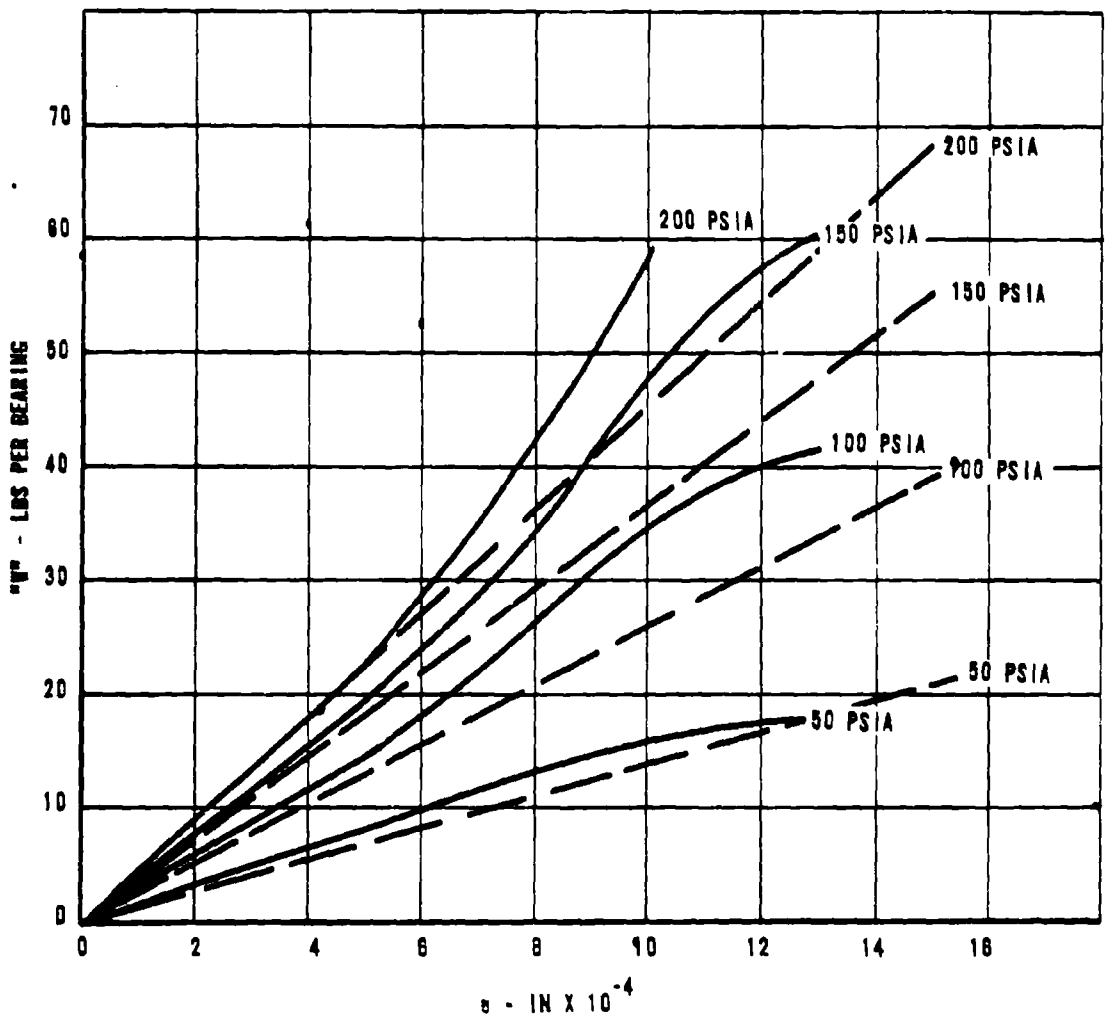

FIG. 19

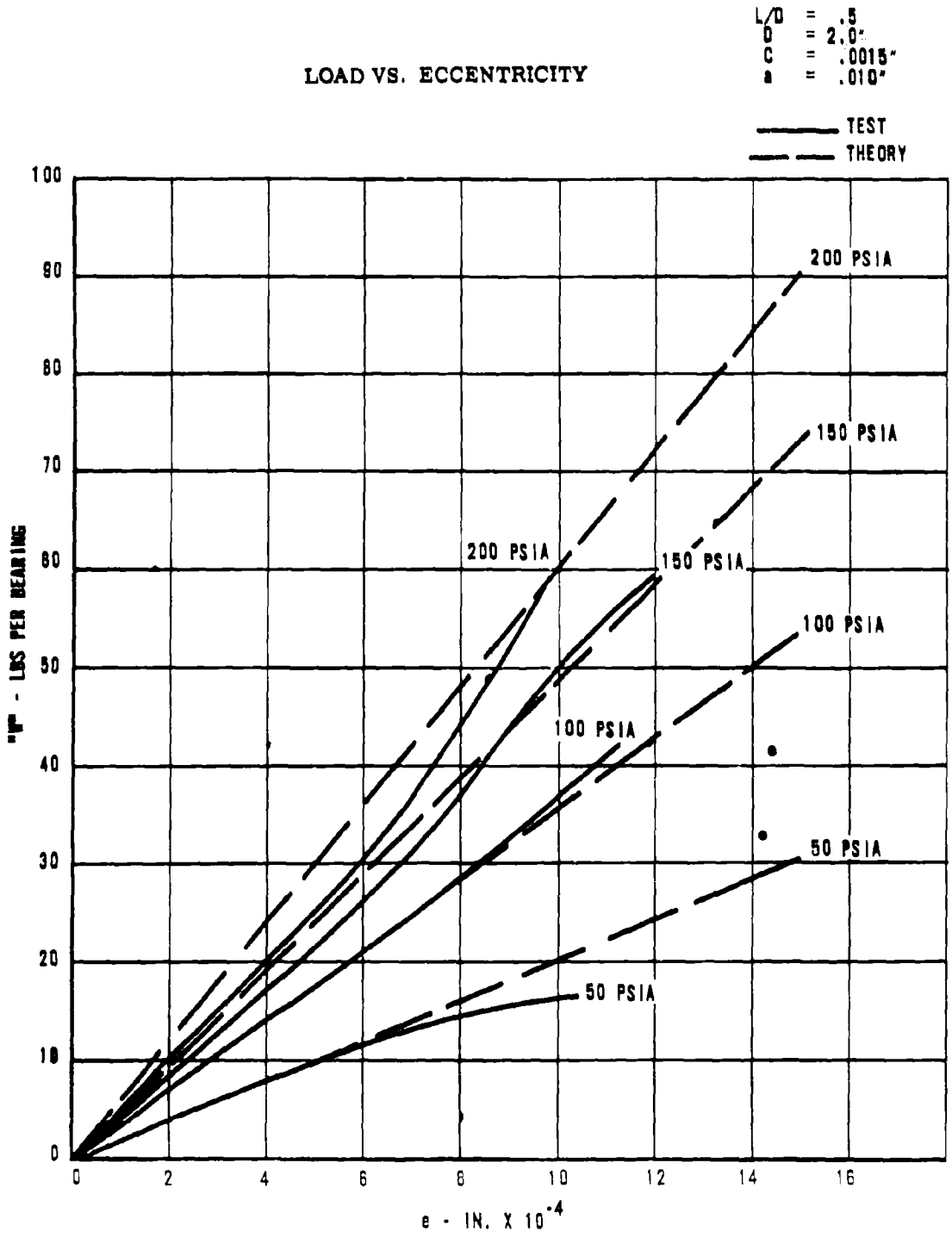
LOAD VS. ECCENTRICITY
L/D = .5
D = 2.0"
C = .0015"
a = .010"
TEST
THEORY
200 PSIA
150 PSIA
100 PSIA
50 PSIA
200 PSIA
150 PSIA
100 PSIA
50 PSIA
"W" - LBS PER BEARING
e - IN. X 10^-4
0
10
20
30
40
50
60
70
80
90
100
0
2
4
6
8
10
12
14
16

FIG. 20

LOAD VS. ECCENTRICITY

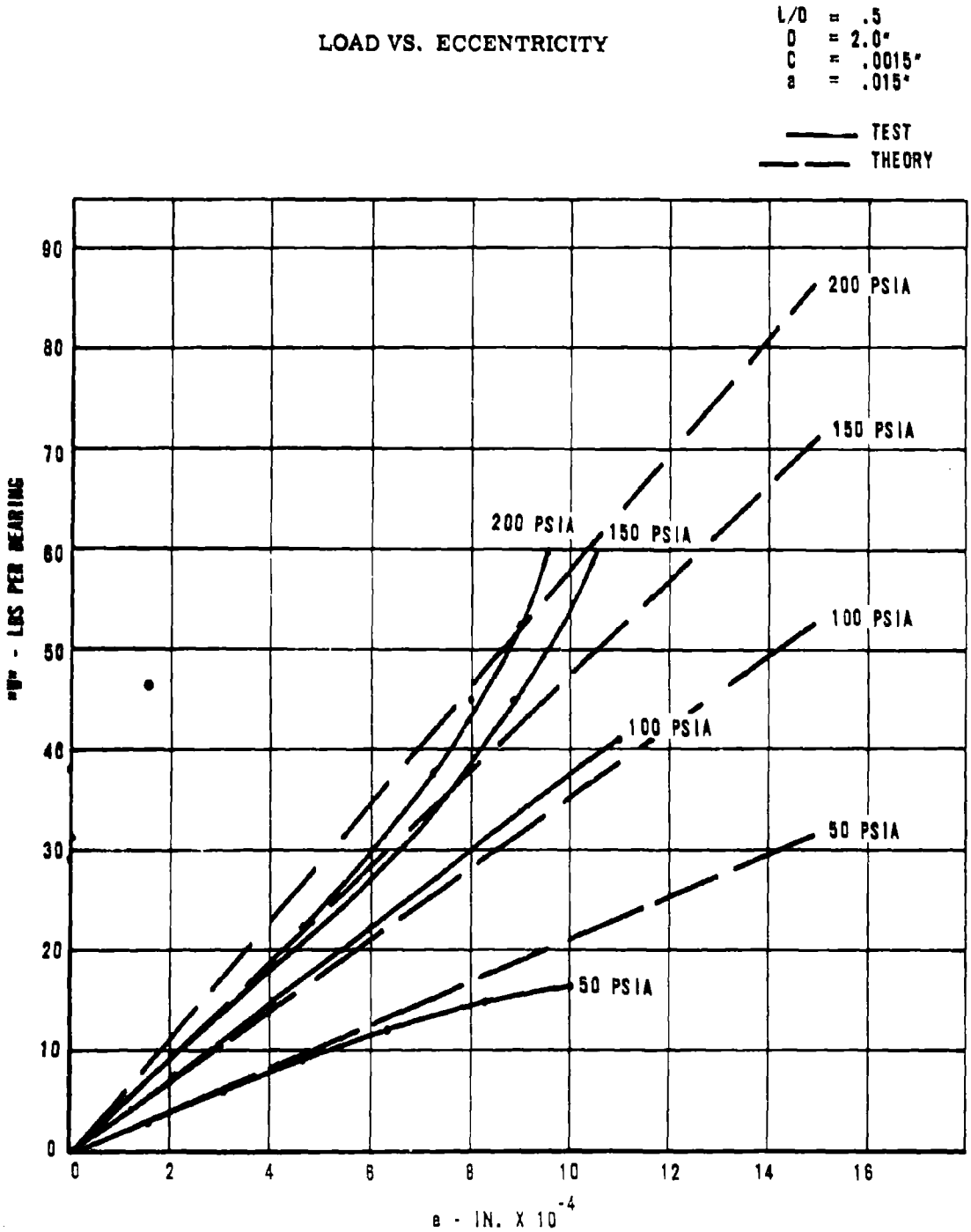

FIG. 21

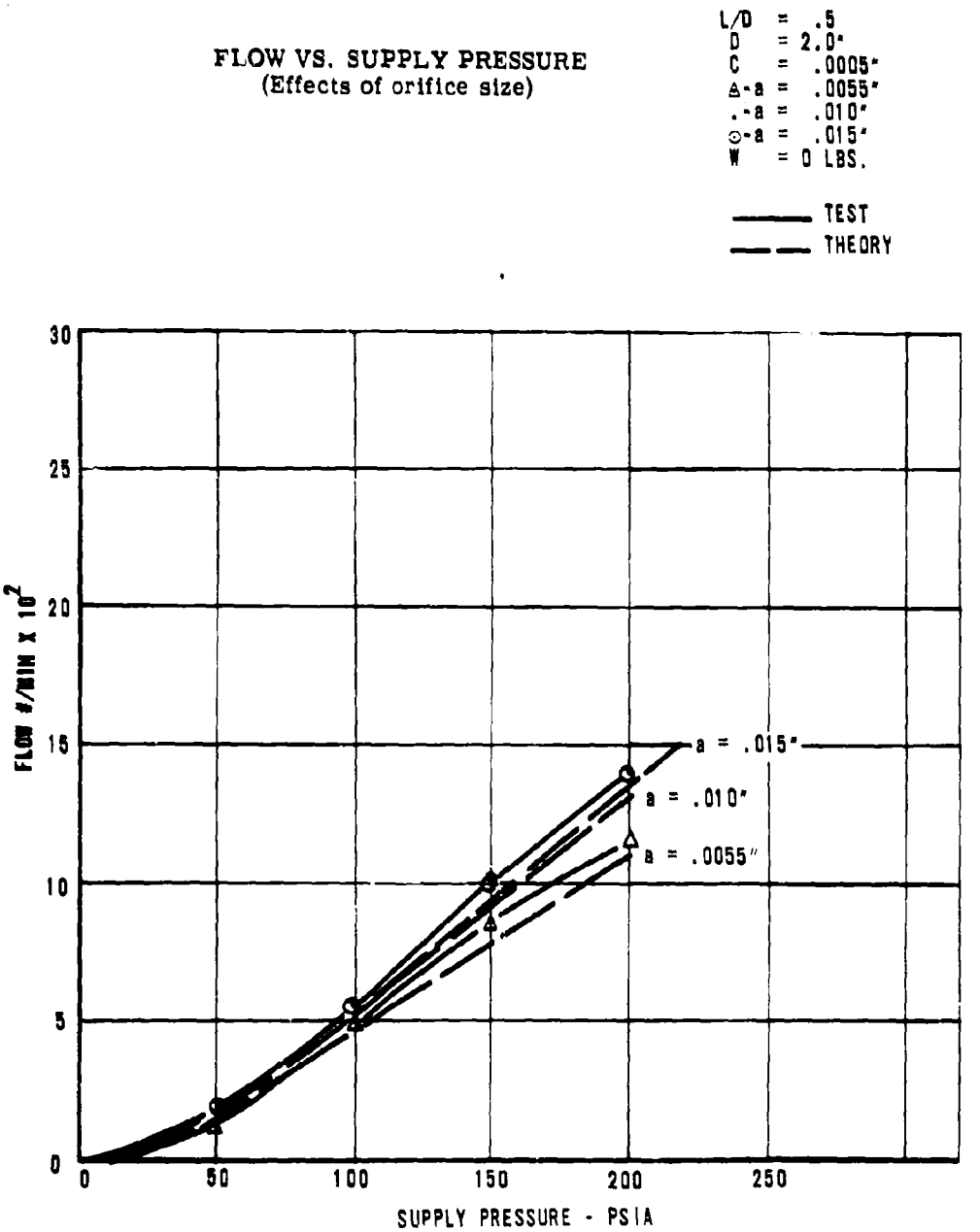
FLOW VS. SUPPLY PRESSURE
(Effects of orifice size)
L/D = .5
D = 2.0"
C = .0005"
△-a = .0055"
.-a = .010"
⊙-a = .015"
W = 0 LBS.
TEST
THEORY
FLOW #/MIN X 10²
SUPPLY PRESSURE - PSIA
a = .015"
a = .010"
a = .0055"
0
5
10
15
20
25
30
0
50
100
150
200
250

FIG. 22

FLOW VS. SUPPLY PRESSURE
(Effects of orifice size)

L/D = .5
D = 2.00"
△-a = .0055"
.-a = .010"
⊙-a = .015"
C = .001"
W = 0 LBS.

——— TEST
— — — THEORY

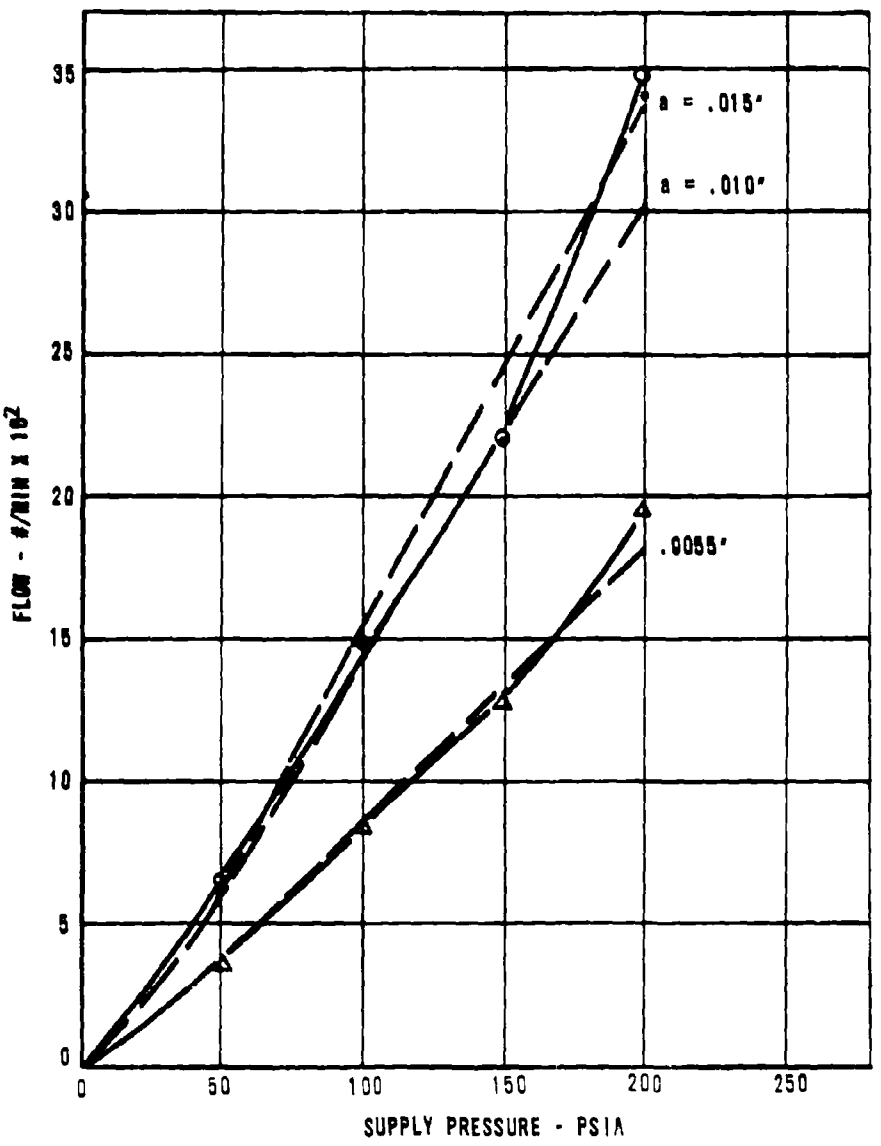

FIG. 23

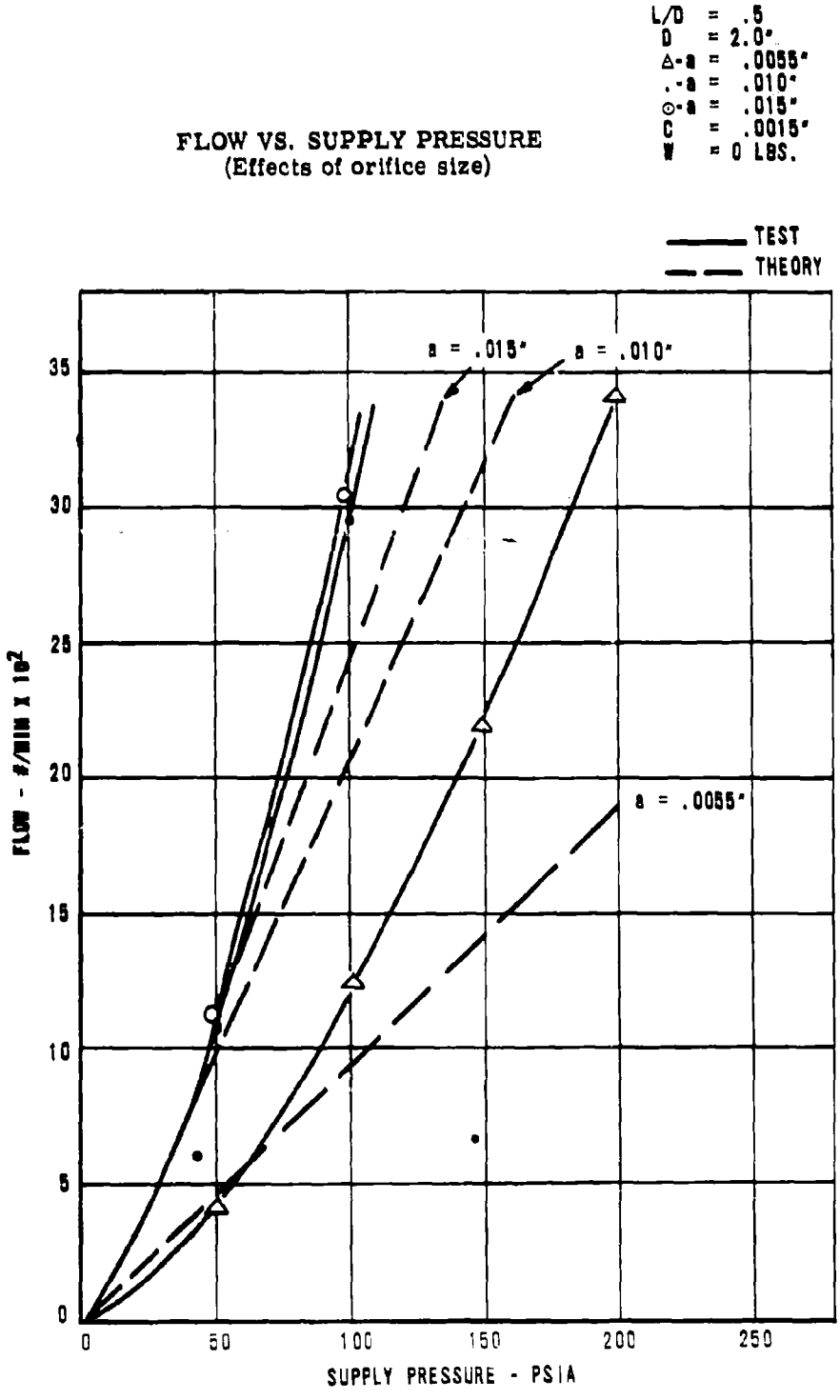
L/D = .5
D = 2.0"
△-a = .0055"
.-a = .010"
⊙-a = .015"
C = .0015"
W = 0 LBS.
FLOW VS. SUPPLY PRESSURE
(Effects of orifice size)
TEST
THEORY
a = .015"
a = .010"
a = .0055"
FLOW - #/MIN X 10²
SUPPLY PRESSURE - PSIA
0
5
10
15
20
25
30
35
0
50
100
150
200
250

FIG. 24

EFFECTS OF SPEED ON FLOW

L/D = .5
D = 2.0"
C = .001"
W = 6.57 LBS.
△-a = .0055"
.-a = .010"
○-a = .015"

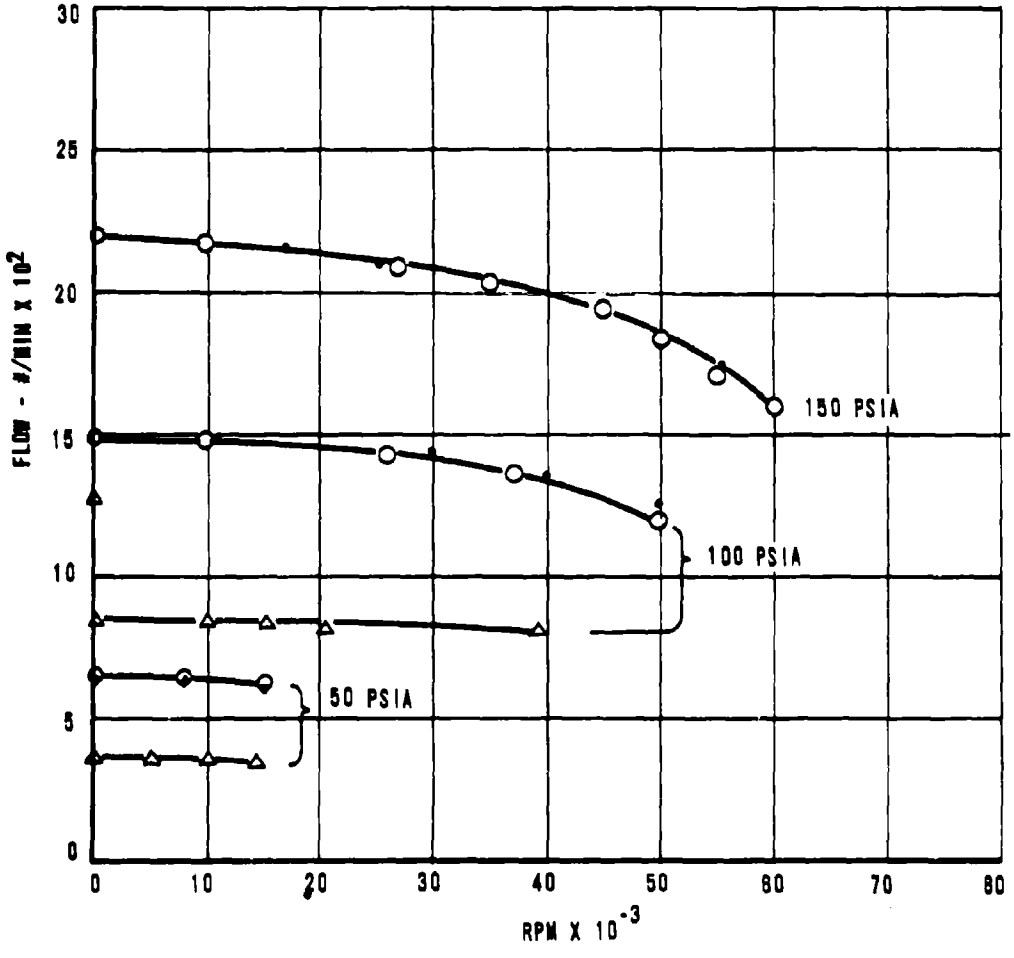

FIG. 25

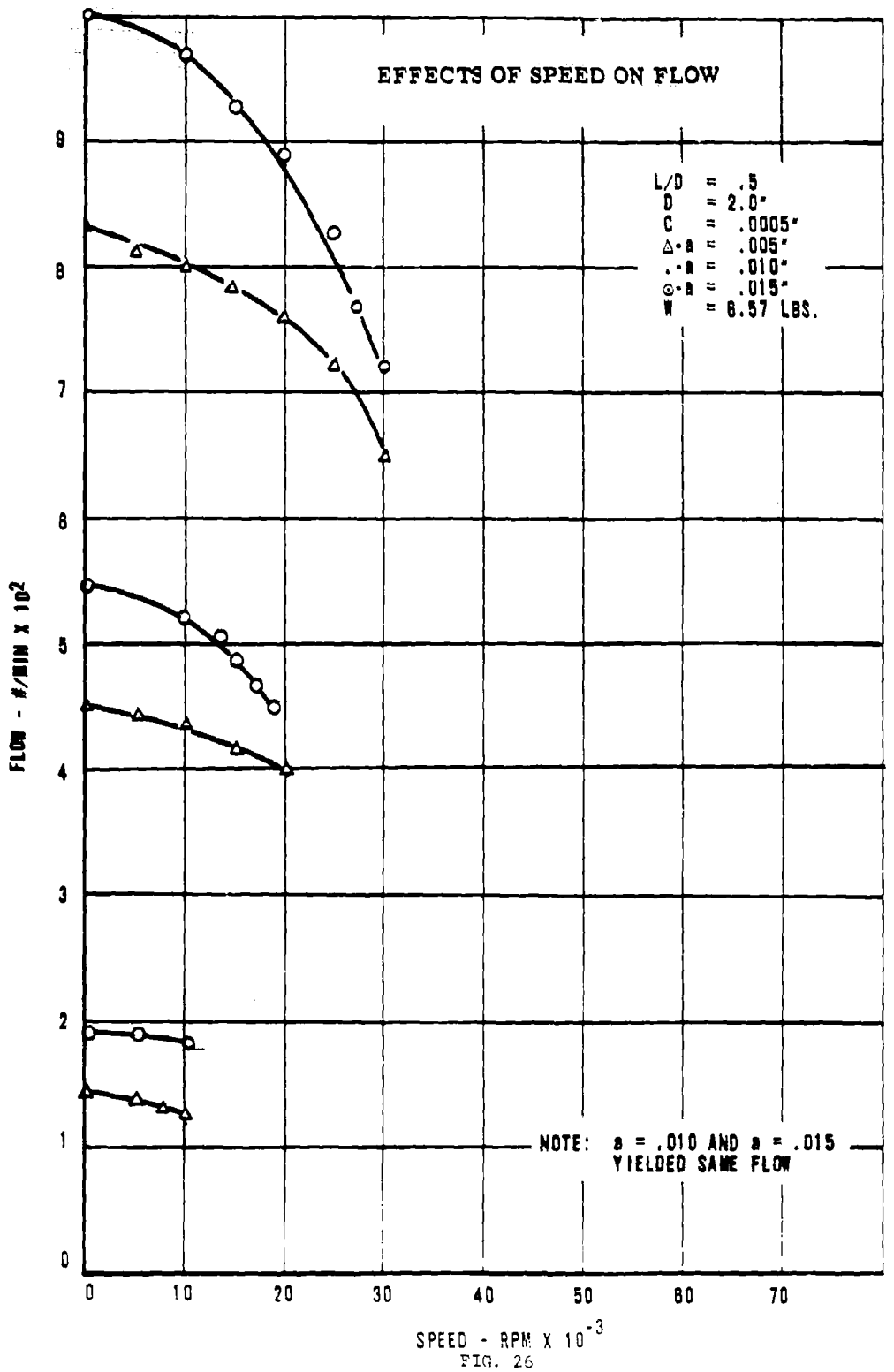
EFFECTS OF SPEED ON FLOW
L/D = .5
D = 2.0"
C = .0005"
△-a = .005"
.-a = .010"
⊙-a = .015"
W = 6.57 LBS.
NOTE: a = .010 AND a = .015 YIELDED SAME FLOW
FLOW - #/MIN X 10²
SPEED - RPM X 10⁻³
0
1
2
3
4
5
6
7
8
9
0
10
20
30
40
50
60
70

FIG. 26

APPROVED DISTRIBUTION LISTS FOR UNCLASSIFIED TECHNICAL REPORTS ISSUED UNDER GAS LUBRICATED BEARINGS CONTRACTS

Contract NONR 2844(00) NR 097-348

Chief of Naval Research
Department of the Navy
Washington 25, D.C.
Attn: Code 438 — 10
461 — 1
423 — 1
429 — 1
463 — 1
466 — 1

Commanding Officer
Office of Naval Research
Branch Office
346 Broadway
New York 13, New York — 1

Commanding Officer
Office of Naval Research
Branch Office
1030 East Green Street
Pasadena 1, California — 1

Commanding Officer
Office of Naval Research
Branch Office
Tenth Floor
The John Crerar Library Bldg.
86 East Randolph Street
Chicago, Illinois — 1

Commanding Officer
Office of Naval Research
Branch Office
Navy No. 100 Fleet Post Office
New York, New York — 10

Office of Naval Research
Resident Representative
University of Pennsylvania
Room 213, Hare Building
Philadelphia 4, Pennsylvania — 1

Director
Naval Training Device Center
Sands Point, Port Washington
Long Island, New York — 1

Chief, Bureau of Ships
Department of the Navy
Washington 25, D.C.
Attn: James C. Reid (Code 644B) — 8

Material Laboratory Library
Building 291, Code 912B
New York Naval Shipyard
Brooklyn 1, New York — 1

Director
Naval Research Laboratory
Washington 25, D.C.
Attn: Code 5230 — 1
2000 — 6

Director
U.S. Naval Engrg. Experiment Station
Annapolis, Maryland
Attn: Supervisor, Bearings Project,
Code 790 — 2

Commanding Officer
U.S. Naval Boiler and Turbine Lab.
Naval Base
Philadelphia, Pennsylvania — 1

Commanding Officer
U.S. Naval Avionics Facility
Indianapolis 18, Indiana
Attn: J.G. Weir — 1

Superintendent
U.S. Naval Postgraduate School
Monterey, California — 1

Commanding General
U.S. Army Engineer R and D Labs.
Fort Belvoir, Virginia
Attn: W.M. Crim, Nuclear Power
Field Office — 2
Technical Intelligence Br. — 1

Office of Chief of Ordnance
Research and Development Division
Department of the Army
Washington 25, D.C.
Attn: Normal L. Kleir — 1

Chief, Bureau of Naval Weapons
Department of the Navy
Attn: G. D. Norman (RAAE-343) 3
L. Schlesinger (RREN-4) 3

Chief of Research and Development
Office, Chief of Staff
Department of the Army
Pentagon Building
Washington 25, D. C. 1

Commanding Officer
U.S. Army Research Office
(DURHAM)
Box CM, Duke Station
Durham, North Carolina 1

Commanding Officer
Detroit Arsenal
Centerline, Michigan
Attn: ORD MX-ECPD 1

Commander
Army Rocket and Guided Missile
Agency
Redstone Arsenal, Alabama
Attn: Technical Library,
ORDXR-OTL 1

Committee on Equipment and
Supplies
Office of the Assistant Secretary
of Defense (R and D)
The Pentagon
Washington 25, D. C. 1

Armed Services Technical
Information Agency
Arlington Hall Station
Arlington 12, Virginia
Attn: TIPCR 10

Commander
Aeronautical Systems Division
of the AirForce Systems Command
Wright Patterson AF Base, Ohio
Attn: WWRMFP-1, W. H. Biedenbender 1
WWRMPF-2, G. A. Beane 1
WWRMDD, P. C. Hanlon 1
ASRCEF-2, J. L. Morris 2

Headquarters
Wright Air Development Division
Air Research and Development Command
United States Air Force
Wright-Patterson AF Base, Ohio
Attn: WWRNGC-k, Phil Eignor 1

Commander
Air Force Office of Scientific
Research
Washington 25, D. C.
Attn: Joseph E. Long (SRDA) 3

Director
National Aeronautics and Space
Administration
1512 H Street, N. W.
Washington 25, D. C.
Attn: Harold Hessing 2

Chief of Staff, U.S. Air Force
The Pentagon
Washington 25, D. C.
Attn: DCS/D AFDRD/AD-2 1
DCS/D AFOP-OO 1

Commander
Air Research and Development Command
Andrews Air Force Base
Washington 25, D. C.
Attn: Lt. Col. C. D. Reifstech, RADTAP 1

Army Reactors Branch
Reactor Development Division
U.S. Atomic Energy Commission
Washington 25, D. C.
Attn: Mr. Clarence Miller 2

Technical Library
U.S. Atomic Energy Commission
Washington 25, D. C.
Attn: John L. Cook 3

Office of Maritime Reactors
Division of Reactor Development
Atomic Energy Commission
Washington 25, D. C.
Attn: Mr. S. Shiozawa 1

Chief, Division of Engineering
Maritime Administration
GAO Building
Washington 25, D. C.

General Engineering Laboratory
General Electric Company
One River Road
Schenectady 5, New York
Attn: Dr. G.M. Rentzepis 1

General Motors Corporation
Research Laboratories Division
Technical Center
Detroit 2, Michigan
Attn: Mr. Robert Davies
Asst. Supr of Bearings
Section 1

Grumman Aircraft Engineering Corp.
Bethpage, Long Island, New York
Attn: Mr. John Karanik, Chief
Systems Design Department 1

Illinois Institute of Technology
Chicago 16, Illinois
Attn: Prof. L.N. Tao 1

International Business Machine Corp.
Research Laboratory
San Jose, California
Attn: Dr. W.A. Gross 5

Franklin Institute
Laboratory for Research and Development
Philadelphia, Pennsylvania
Attn: Professor D.D. Fuller 5

International Telephone and
Telegraph Laboratories
15151 Bledsoe Street
San Fernando, California
Attn: Mr. G.B. Speen 1

Institute of Aeronautical Sciences
2 East 64th Street
New York, New York 1

Jack and Heintz, Inc.
207 East Laboratory, Public Roads Bldg.
Washington National Airport
Washington 1, D.C. 1

Kearfott Company
1378 Main Street
Clifton, New Jersey
Attn: Mr. Walter Carow 1

Koppers Company, Inc.
Metals Products Division
P.O. Box 626
Baltimore, Maryland
Attn: Mr. I.C. Kuchler 1

Lear, Incorporated
Grand Rapids Division
110 Ionia Avenue, N.W.
Grand Rapids 2, Michigan 1

Lear, Incorporated
3171 South Bundy Drive
Santa Monica, California
Attn: Richard M. Mock, President 1

Litton Industries
336 North Foothill Road
Beverly Hills, California
Attn: Mr. D. Moors, Dept. 21 1

Lockheed Aircraft Corporation
Missiles and Space Division
P.O. Box 504
Sunnyvale, California
Attn: Dr. M.A. Steinberg, 53-30
Building 202, Plant 2, PA 1

Lycoming Division
Avco Manufacturing Corp.
Main Street
Stratford, Connecticut
Attn: Mr. S.B. Withington
President and General Manager 1

McDonnell Aircraft Corporation
Lambert St. - St. Louis Municipal
Airport
Box 516
St. Louis 3, Missouri
Attn: Mr. Kendall Perkins
Vice President (Engr.) 1

Marquardt Aircraft Company
P.O. Box 2013-South Annex
Van Nuys, California
Attn: Mr. A.J. Kreiner, Director
Controls and Accessories Div. 1

Massachusetts Institute of Technology
Room 35-132
Cambridge 39, Massachusetts
Attn: Prof. Milton C. Shaw
Depart. of Mechanical Engrg.

Jet Propulsion Laboratory
California Institute of Technology
4800 Oak Grove Avenue
Pasadena, California
Attn: Engineering Library 1
Dr. John H. Laub

Chief, Technical Information
Service Extension
P.O. Box 62
Oak Ridge, Tennessee
Attn: Melvin S. Day 1/repro

Head, Experimental Engineering,
R.P.D.
Oak Ridge National Laboratory
Building 9201-3
Oak Ridge, Tennessee
Attn: H.W. Savage 1

Commanding Officer
Diamond Ordnance Fuze Laboratories
Washington 25, D.C.
Attn: Technical Reference Section
(ORDTL 06.33) 1

Office, Chief of Engineers
Engineer R and D Division
Gravelly Point
Washington 25, D.C. 1

SP 23-Guidance
U.S. Navy
Washington, D.C.
Attn. D. Gold 2

Office of Technical Services
Department of Commerce
Washington 25, D.C. 1

A.C. Spark Plug Division
General Motors Corporation
Milwaukee 1, Wisconsin
Attn: Allen Knudsen 1

A.C. Spark Plug Division
General Motors Corporation
Route 128
Wakefield, Massachusetts
Attn: W.H. St. Laurent 1

Aerojet-General Corporation
Nucleonics
San Ramon, California 1

AiResearch Manufacturing Division
The Garrett Corporation
9851 S. Sepulveda Boulevard
Los Angeles, California
Attn: Jerry Glaser, Supervisor
Mechanical Lab. Dept. 93-17 1

Allis Chalmers Manufacturing Co.
Buda Division
1126 South 70th Street
Milwaukee 1, Wisconsin
Attn: Mr. Will Mitchell, Jr.
Acting Director of Research
Research Division 1

American Society of Lubrication Engrgs.
5 North Wabash Avenue
Chicago 2, Illinois 1

Chairman, Research Committee on
Lubrication
American Society of Mechanical Engrs
29 West 39th Street
New York 18, N.Y. 1

Analogue Controls, Inc.
200 Frank Road
Hicksville, L.I., New York
Attn: Mr. J.L. Cherubim
Chief Engineer 1

Applied Physics Laboratory
Johns Hopkins University
Silver Spring, Maryland
Attn: George L. Seielstad,
Supr, Tech. Reports Group 1

Autonetics
A Division of N. American Aviation
9150 East Imperial Highway
Downey, California 1

The Barden Corporation
Danbury, Connecticut
Attn: B.L. Mims, Vice President 1

Battelle Memorial Institute
505 King Avenue
Columbus 1, Ohio
Attn: Dr. Russell Dayton 1

Beemer Engineering Company
401 North Broad Street
Philadelphia 8, Pa. 1

Maico Electronics, Inc.
21 North Third Street
Minneapolis 1, Minnesota
Attn: Mr. G.E. Adams
Automatic Controls Dept. 1

Massachusetts Institute of Technology
Department of Aeronautical Engineering
Instrumentation Laboratory
Cambridge 39, Massachusetts 2

Dynamic Analysis and Control Lab.
Massachusetts Institute of Technology
Cambridge 39, Massachusetts
Attn: Dr. R.W. Mann 1

Aeronautical Engineering Labs.
University of Michigan
Ann Arbor, Michigan
Attn: Prof. R.B. Morrison 1

Minneapolis-Honeywell Regulator Co.
Gyro Section
2600 Ridgeway Road
Minneapolis, Minnesota
Attn: Mr. Jack W. Lower
Chief, Aeronautical Div. 1

Cryogenic Engineering Laboratory
National Bureau of Standards
Boulder, Colorado
Attn: Mr. B.W. Birmingham 1
Library 1

U.S. Department of Commerce
National Bureau of Standards
Boulder Laboratories
Boulder, Colorado 1

New Departure
Division of General Motors Corp.
Briston, Connecticut
Attn: R.N.S. Schiedt, Manager
Bearing Development and Contract 1

Norden Laboratories
Norden Div. of United Aircraft Corp.
White Plains, New York
Attn: Miss Elizabeth Zeil, Librarian 1

Department of Chemical Engineering
New York University
New York 53, New York
Attn: James J. Barker, Assoc. Prof.
of Nuclear Engineering

New Hampshire Ball Bearings, Inc.
Peterborough, New Hampshire
Attn: Mr. Henry F. Villaume, Engr. 1

Northrop Corporation
Norair Division
1001 East Broadway
Hawthorne, California
Attn: Library, 3145-31 1

Nortronics
A Division of Northrop Corporation
100 Morse Street
Norwood, Massachusetts
Attn: Mr. E.L. Swainson, Tech. Asst.
Precision Products Dept. 1

The Technological Institute
Northwestern University
Evanston, Illinois
Attn: Professor A. Charnes 1

Pratt and Whitney Aircraft Div. CANEL
P.O. Box 1102
Middletown, Connecticut 1

Radio Corporation of America
Camden, New Jersey 1

Ryan Aeronautical Company
Lindberg Field
San Diego 12, California
Attn: Mr. Frank W. Fink
Vice Pres. and Chief Engr. 1

Sanderson and Porter
72 Wall Street
New York 5, New York
Attn: Mr. S.T. Robinson

Solar Aircraft Company
2200 Pacific Highway
San Diego 12, California
Attn: Paul A. Pitt, Chief Engineer 1

Space Technology Laboratories, Inc.
P.O. Box 95001
Los Angeles 45, California
Attn: Mr. Kenton Andrews
Bldg. "F", Room 125 1

Sperry Gyroscope Company
Div. Of Sperry Rand Co.
Great Neck, L.I., New York
Attn: Mr. Wilmer L. Borrow
Vice President for R and D

Utica Division
Bendix Aviation Corporation
Utica, New York
Attn: Mr. Russell T. DeMuth,
Senior Engr. 1

Bendix Aviation Corporation
Research Laboratories Division
Southfield, Michigan
Attn: Mr. Ralph H. Larson 1

Boeing Airplane Company
Research Group
Box 3707
Seattle 25, Washington
Attn: Mr. D.J. Melchior
Mechanical Equipment 1

Bryant Chucking Grinder Company
60 Clinton Avenue
Springfield, Vermont
Attn: Mr. Roald Cann 1

Cadillac Gage Company
P.O. Box 3806
Detroit 5, Michigan
Attn: Mr. J. Taylor, Project Engr. 1

Carrier Corporation
Division of Research
Research Center
Syracuse, New York
Attn: Dr. Dewey J. Sandell 1

Chance Vought Corporation
P.O. Box 5907
Dallas, Texas
Attn: Mr. R.C. Blaylock
Vice President, (Engr) 1

Chrysler Corporation
Defense Operations
P.O. Box 757
Detroit 31, Michigan
Attn: Mr. C.W. Snider 1

The Cleveland Graphite Bronze Co.
17000 St. Clair Avenue
Cleveland 10, Ohio
Attn: Mr. R.H. Josephson 1

Collins Construction Co.
P.O. Box 86
Port Lavaca, Texas
Attn: Mr. James D. Mamarchev
Consulting Engineer 1

Convair
A Division of General Dynamics Corp.
Fort Worth, Texas
Attn: Mr. L.E. McTaggart, Sr.Des.Engr.
Engrg. Annex No. 1 1

Curtiss-Wright Corp.
Wright Aeronautical Division
Department 8311
Wood Ridge, New Jersey
Attn: Mr. W.J. Derner,
Chief Project Engr. 1

Daystrom Pacific
9320 Lincoln Boulevard
Los Angeles 45, California
Attn: Robert H. Smith
Special Project Engr. 1

Dynamic Controls Corporation
14 Runde Lane
Bloomfield, Connecticut
Attn: Mr. Thomas P. Farkas 1

E.I. DuPont de Nemours and Co., Inc.
Wilmington 98, Delaware
Attn: Dr. McNeilly
Mechanical Development Lab. 1

Electronics Systems Laboratory
Federal Telecommunications Labs.
Nutley, New Jersey
Attn: Mr. John Metzger 1

Ford Instrument Co.
31-10 Thomson Avenue
Long Island City 1, New York
Attn: Mr. Jarvis

Ford Motor Company
Dearborn, Michigan
Attn: Prof. Adolph Egli 1

General Atomics Division
General Dynamics Corp.
P.O. Box 608
San Diego 12, California
Attn: Mr. F.W. Simpson 1

General Engineering Laboratory
General Electric Company
One River Road
Schenectady 5, New York
Attn: Dr. Beno Sternlicht

Sperry Gyroscope Company
1 x 115
Great Neck, L.I., New York
Attn: Mr. John W. Steves 1

Stevens Institute of Technology
Hoboken, New Jersey
Attn: Prof. P.F. Martinuzzi 1

Stratos Division
Fairchild Airplane and Engine Co.
Bay Shore, L.I., New York
Attn: Mr. George Mackowski 1

Sundstrand Turbo
2480 West 70th Avenue
Denver 21, Colorado 1

Thompson Ramo Wooldridge Corporation
P.O. Box 90534 Airport Station
Los Angeles 45, California
Attn: Mr. Robert I. King F1829 1

AiResearch Mfg. Co. of Arizona
P.O. Box 5217
Phoenix, Arizona
Attn: Librarian 2

Waukesha Bearings Corporation
P.O. Box 346
Waukesha, Wisconsin
Attn: Mr. J.M. Gruber, Ch. Engr. 1

Tribo-Netics Laboratories
Vermilion, Ohio
Attn: Mr. E. Fred Macks 1

Universal Match Company
Avionics Dept. Technical Library
4407 Cook Avenue
St. Louis 13, Missouri 1

USI Technical Center
3901 N.E. 12th Avenue
Pompano Beach, Florida
Attn: Dr. W.C. Knopf 1

School of Mechanical Engineering
University of Pennsylvania
Philadelphia 4, Pennsylvania
Attn: Prof. P.R. Trumpler, Director 1

Westinghouse Electric Corporation
Research Laboratories
East Pittsburg, Pennsylvania
Attn: Mr. John Boyd

Westinghouse Electric Corporation
P.O. Box 868
Pittsburg 30, Pennsylvania
Attn: Mr. J.K. Hardnette
Vice Pres. and General Manager 1

Worthington Corporation
Harrison, New Jersey
Attn: Mr. H. Walter
Director of Research 1

Litton Industries
336 North Foothill Road
Beverly Hills, California
Attn: Dr. J.S. Ausman 2